INSTITUTO POLITÉCNICO DE BRAGANÇA Escola Superior Agrária

Dual-aptasensor array for osteopontin detection: optimization of aptamers immobilization conditions

Maha Ezziddine

Dissertation Presented to the Polytechnic Institute of Bragança to obtain the Master Degree in Biotechnological Engineering

Supervisors

Professor Dr. António Manuel Coelho Lino Peres

Professor Dr. Ali Othmane

Dra. Sofia Gabriel Meirinho

Bragança

2017

INSTITUTO POLITÉCNICO DE BRAGANÇA Escola Superior Agrária

المعهد العالي للبيوتكنولوجيا بالمنستير
INSTITUT SUPERIEUR DE BIOTECHNOLOGIE DE MONASTIR

Dissertation made under the agreement of Double Diploma between the Escola Superior Agrária de Bragança / IPB and the High Institut of Biotechnology of Monastir / ISBM, Tunisia to obtain the Degree of Master in Biotechnological Engineering.

Preface and Acknowledgements

Praise be to God, the most merciful and the most gracious. Without his blessing my accomplishment would never have been possible.

The research work in this dissertation was fulfilled at the school of Agrária of the Polytechnic Institute of Bragança (IPB), Portugal. The financial support from the International Credit Mobility (ICM) project and from Project POCI-01–0145-FEDER-006984 – Associate Laboratory LSRE-LCM funded by FEDER - Fundo Europeu de Desenvolvimento Regional through COMPETE2020 - Programa Operacional Competitividade e Internacionalização (POC) – and by national funds through FCT - Funda o para a Ciência e a Tecnologia, Portugal, is acknowledged.

The completion of this dissertation would not have been possible without the technical and emotional support of many individuals. I would like to take this opportunity to express my deep gratitude to all these persons.

First, I would like to thank my supervisor Professor Dr. António Manuel Coelho Lino Peres and my co-supervisor PhD. Sofia Gabriel Meirinho. Their guidance, valuable comments, understanding, patience, active involvement, and constant support during the course of my dissertation helped me a lot to obtain fruitful outcomes. I want to express also my gratitude to my Tunisian co-supervisor Professor Dr. Ali Othmane for his encouragement and support.

My sincere gratitude goes to the all teaching and non-teaching staff of the Polytechnic Institute of Bragança. It was really a great opportunity for me to be your student.

My special thanks go to all of my friends and schoolmates for their friendly support at many occasions during my stay in Bragança.

Last but not least, I would like to express my endless gratefulness to my family for their commitment, sacrifice, and support throughout my life in general and during my studies in particular.

Abstract

Cancer diseases are associated with the presence of several protein biomarkers. Aptasensor arrays may allow early multiple-detection of these biomarkers which can make significant improvements in the lives of cancer patients. Clinical studies suggest that osteopontin, an overexpressed protein by tumor cells, may be used as a diagnostic biomarker for various cancers. The aim of the present work was to establish the optimal experimental conditions that allow enhancing the performance of an electrochemical dual-aptasensor array for the detection of osteopontin. The aptamer concentration, time and temperature of immobilization into the dual-screen printed gold electrodes (Dual-SPGE) as well as the aptamer-protein interaction time were evaluated using a 2^k factorial experimental design. DNA and/or RNA aptamers were immobilized on the Dual-SPGE via streptavidin-biotin interaction and the evaluation of the best experimental conditions was carried out by cyclic and square wave voltammetry using a ferro/ferricyanide solution ($[Fe(CN)_6]^{3-/4-}$) as a redox probe. Statistical significant models for both DNA and RNA aptamers were established. Temperature and aptamer concentration were found to be the most significant parameters. Also, the results pointed out that interaction effects between the four parameters were usually statistically significant, showing that there was a dependency between aptamer concentration-aptamer immobilization time and between temperature-aptamer immobilization time. The optimum experimental conditions found for enhancing the performance of the dual-aptasensor array were 4°C, 0.5 µM of aptamer concentration, 20 min of aptamer incubation and 30 min of aptamer-osteopontin interaction.

Resumo

O cancro é uma doença à qual pode ser associada a presença de diversas proteínas nos fluidos biológicos de pacientes com essa patologia, as quais podem ser usadas como biomarcadores. Os biossensores à base de vários aptâmeros (aptasensors arrays) podem permitir a deteção múltipla desses biomarcadores num estágio precoce da doença, podendo proporcionar melhorias significativas na vida dos pacientes com cancro. Estudos clínicos sugerem que a osteopontina, é uma proteína sobre-expressa por células tumorais, podendo ser utilizada como biomarcador no diagnóstico de vários tipos de cancro. O objetivo do presente trabalho foi estabelecer as condições experimentais que maximizassem o desempenho de um duplo biossensor eletroquímico contendo dois aptâmeros (duplo-aptasensor array) para a deteção de osteopontina. O desenho experimental 2^k fatorial foi utilizado com o intuito de estudar o efeito da concentração dos aptâmeros, tempo e a temperatura de imobilização no elétrodo de trabalho de ouro duplo (duplo-SPGE), bem como o tempo de interação aptâmero-proteína. Os aptâmeros de ADN e/ou ARN foram imobilizados no duplo-SPGE através da interação biotina-estreptavidina e a avaliação das melhores condições experimentais foi realizada por voltametria cíclica e voltametria de onda quadrada usando uma solução de ferro/ferricianeto ($[Fe(CN)_6]^{3-/4-}$) como solução redox. Para os aptâmeros de ADN e ARN foram estabelecidos modelos significativos, sendo a temperatura e a concentração dos aptâmeros os parâmetros mais significativos. Além disso, os resultados mostraram que o efeito da interação dos 4 parâmetros foi em geral estatisticamente não significativo, verificando-se uma dependência do tempo de imobilização dos aptâmeros com a concentração dos aptâmeros e com a temperatura aplicada, respetivamente. As condições experimentais ótimas estabelecidas de forma a melhorar o desempenho do duplo-aptasensor array foram uma temperatura de 4ºC, com uma concentração de 0.5 μM para dois aptâmeros, após 20 min e 30 min de incubação no duplo-SPGE e de interação aptâmeros-osteopontina, respetivamente.

Résumé

Les maladies cancéreuses sont liées à plusieurs biomarqueurs protéiques qui peuvent être précocement détectés par des biocapteurs à aptamères et par conséquent des améliorations notables peuvent être apportées à la vie des patients. Des études cliniques suggèrent que l'ostéopontine, une protéine surexprimée par les cellules tumorales, peut être utilisée comme un biomarqueur pour le diagnostic du cancer. Le but du présent travail est d'établir les conditions expérimentales optimales permettant d'améliorer la performance d'un biocapteur éléctrochimique à deux aptamères pour la détection de la protéine ostéopontine. La concentration de l'aptamère, la température et le temps d'immobilization de l'aptamère sur une électrode en or imprimée par sérigraphie ainsi que le temps d'interaction aptamère-protéine ont été évalués en suivant un plan factoriel à deux niveaux. Les aptamères ont été immobilisés sur l'électrode via une interaction streptavidine-biotine et l'évaluation des meilleures conditions expérimentales a été effectuée par voltammetrie cyclique et par voltampérométrie à impulsion rectangulaire en utilisant une solution de ferro/ferricyanure ($[Fe(CN)_6]^{3-/4-}$) comme sonde redox. Des modèles statistiquement significatifs relatifs aux aptamères d'ADN et d'ARN ont été établis. La température et la concentration de l'aptamère ont été les paramètres les plus significatifs. L'effet des interactions entre les quatre paramètres a montré qu'il existe une dépendance entre la concentration de l'aptamère et le temps d'immobilisation de l'aptamère et entre la température et le temps d'immobilisation de l'aptamère. Les conditions expérimentales optimales pour améliorer la performance du biocapteur étaient 20 minutes d'incubation d'aptamère, 30 minutes d'interaction aptamère-ostéopontin, une température d'incubation de 4°C et une concentration d'aptamère de l'ordre de 0,5 μM.

TABLE OF CONTENTS

LIST OF FIGURES

LIST OF TABLES

LIST OF OF SYMBOLY AND ABBREVIATIONS

ΔEp - potential variation between cathodic and anodic peaks

Δ*I* - relative current change

AE - auxiliary electrode

Ag/AgCl - silver/silver chloride

ANOVA - analysis of variance

CA - cancer antigen

CV - cyclic voltammetry

DEPC - diethypyrocarbonate

DNA - deoxyribonucleic acid

DPA - 3,3'-dithiodipropionic acid

EDC - N-(3-dimethylaminopropyl)-N-ethylcarbodiimide hydrochloride

ELISA - enzyme-linked immunosorbent assays

ETA - ethanolamine

FDA - Food and Drug Administration

HCC - hepatocellular carcinoma

HE42 - Human epididymis protein

*I*p - peak current intensity

*I*pa - anodic peak current

*I*pc - cathodic peak current

KCl - potassium chloride

K_d - dissociation constants

KH_2PO_4 - potassium dihydrogen phosphate

LSD - least significant difference

MMPs - matrix metalloproteinases

NaCl - sodium chloride

NHS - N-hydroxysuccinimide

OFAT- one-factor-at-a-time

ox- oxydation

PSA - prostate-specific antigen

Pro2PSA1 - pro-prostate specific antigen

RE - reference electrode

red - reduction

RNA - ribonucleic acid

SAMs - self-assembled monolayers

SELEX - Systematic Evolution of Ligands by Exponential Enrichment

SPGEs - screen-printed gold electrodes

SPSS - Statistical Package for Social Sciences

SWV - square wave voltammetry

uPA - urokinase plasminogen activator

WE - working electrode

CHAPTER 1

Context, aims and thesis Outline

1.1. Context and motivation

Proteins are a major class of cancer biomarkers and depending on the concentration levels (high or low) they may be used as diagnostic markers (Song et al. 2014). Osteopontin, as an example of protein biomarker that is involved in all the stages of cancer progression, may play an essential role in clinical prognosis and diagnosis (Shevde & Samant 2014; Ahmed et al. 2011). Thus, nowadays, the development of reliable, sensitive, cost-effective, and specific strategies for detecting and quantifying disease-related proteins is of particular importance. Based on the antigen−antibody reaction, immunological assays are the most commonly used diagnostic methods for protein detection (Li et al. 2016). However, in some cases, the immune assay is faced with several considerable challenges and drawbacks such as the requirement of specific antibodies, the need of large amounts of samples, and long response times (Chatziharalambous et al. 2016; Li et al. 2016; Meirinho 2016). Recently, biorecognition elements based on aptamer−protein interaction have gained more attention. Aptamers, which are short, single-stranded DNA or RNA able to recognize many targets including proteins, possess several features that make them a more effective choice than antibodies for diagnostic purposes (Lowe 2008; Moreno 2014). Compared to other detection methods, aptamer-based electrochemical biosensors attracted more attention because they are more sensitive, more reliable, cheaper and simpler (Meirinho et al. 2015; Arya et al. 2007). However, aptasensors (aptamer-based biosensors) that employ single aptamer as recognition element still have limitations mainly due to the false positive results (Cao et al. 2017). Due to this limited specificity, dual-aptasensor arrays, which comprise two or more different aptamers towards the same or different targets, gained importance, being their usual selectivity acceptable for the early diagnosis of human diseases (Khang et al. 2017). Several parameters influence the performance of the dual-aptasensor array, in particular the incubation temperature, the concentration of aptamers, immobilization time of aptamers and contact time between aptamers and proteins (Meirinho 2016). However, the study of each effect or all effects using a conventional full design would turn out into a quite time consuming task. To overcome this drawback, a 2^k factorial design can be used allowing the simultaneous optimization of all effects and taking into account their possible interactions (Elhalil et al. 2016). Although several aptasensor arrays were developed (Bosco et al. 2013; Bai et al. 2013; Feng et al. 2016; Feng et al. 2015), statistical design of experiments have been only applied in a few studies (Ugo & Moretto

2016). Accordingly, the aim of this work was to establish the optimal experimental immobilization conditions, using 2^k factorial design, in order to develop an electrochemical dual-aptasensor array for the detection of osteopontin with improved analytical performance compared to the known performance of single-aptasensor arrays.

1.2. Research Aims

The purpose of this work is to model the signal response of the developed electrochemical dual-aptasensor array for the detection of osteopontin protein which has been reported as a cancer biomarker and optimize the aptamers' experimental immobilization conditions namely, the aptamer concentration, time and temperature of immobilization into dual-screen printed gold electrodes (Dual-SPGE) and the aptamer-protein interaction time, to have a better signal response using a 2^k factorial design methodology.

The specific objectives included:

1. Development of an electrochemical dual-aptasensor array using a previsoulsy reported RNA and DNA aptamers specific for the target osteopontin.
2. Immobilization of the bioreceptors (RNA and DNA aptamers) onto the Dual-SPGE via streptavidin-biotin interaction for the simultaneous detection of the protein osteopontin.
3. Evaluation of the best experimental conditions by cyclic and squarewave voltammetry using a ferro/ferricyanide solution ($[Fe(CN)_6]^{3-/4-}$) as a redox probe.
4. Study of the effect the type of aptamer and electrochemical technique on the dual-aptasensor response
5. Predict the response of the aptasensor by a first-order model equation.

1.3. Thesis outline

This thesis was structured in five chapters that cover the research aims stated above:

- Chapter 1: Describes the context and motivation of this work, states the research aims, and provides the thesis outline
- Chapter 2: Presents the literature review that supports the thesis work.
- Chapter 3: Lists the materials and methods used in the experimental work as well as the steps followed to establish the 2^k factorial design and to analyze the obtained results.

- Chapter 4: Combines the result section and discussion part into a single chapter. This chapter sets out the experimental results including the statistical analysis, interprets and explains the obtained results and answers the research question.
- Chapter 5: Involves conclusive comments, observations and perspectives for further research on this research subject.

CHAPTER 2

Introduction

2.1. *Cancer: a cluster of diseases*

Cancer is a generic term for a large group of diseases that can affect any part of the body (Bhatt et al. 2010). Unlike normal cells, cancer cells ignore signals that stop cell division and induce cell death process which the body uses to get rid of unneeded, old or damaged cells. As a result, extra cells begin to divide without stopping, form tumors and spread into surrounding tissues (Misek & Kim 2011). This survival advantage and undiminished proliferative potential of cancer cells are caused by alterations in the status and expression of primarily three main classes of genes:

- Proto-oncogenes which are a group of genes encoding for proteins that stimulate cell division, inhibit cell differentiation, and halt cell death. This group of genes is important for normal human development and for the maintenance of tissues and organs. When a proto-oncogene mutates or is highly expressed it turns into an oncogene that can become permanently or activated when it is not supposed to be. When this happens, the cell grows out of control, which can lead to cancer (Lehman et al. 1991).
- Tumor suppressor genes are a cluster of genes encoding for proteins that inhibit cell proliferation by promoting apoptosis and arresting the cell cycle if DNA is damaged. Cells with certain alterations in tumor suppressor genes may divide in an uncontrolled manner (Lee & Muller 2010).
- DNA repair genes, which code for proteins that correct errors arising when cells duplicate their DNA prior to cell division. Mutations in DNA repair genes can lead to a failure in repair, which in turn allows subsequent mutations to accumulate. The accumulation of errors can overwhelm the cell and result in cancer (Wood et al. 2001).

All of these genetic changes happen over a person's lifetime as a result of errors that occur as cells divide or because of damage to DNA caused by certain environmental exposures including physical carcinogens, such as ultraviolet and ionizing radiation, chemical carcinogens (such as components of tobacco smoke and aflatoxins) and biological carcinogens (like infections from certain viruses, bacteria, or parasites) (Clapp et al. 2005). When faulty genes are inherited from parents, the risk of cancer is much more higher (Harris 2015).

In response to cancer, normal cells as well as cancer cells produce substances that can be found in the blood, urine, stool, tumor tissue, or other body fluids (Gam 2012). These substances are called cancer biomarkers. The following section will discuss some important cancer biomarkers.

2.2. Cancer biomarkers

A biomarker is any substance or process that can be objectively measured as an indicator of normal biological processes or pathogenic processes (Henry & Hayes 2012). In cancer, a biomarker refers to a substance or process that is indicative of the presence of cancer in the body (Mishra & Verma 2010). In terms of the usage of biomarkers, cancer biomarkers can be classified into three main categories, namely diagnostic, prognostic and predictive biomarkers (Goossens et al. 2015). A diagnostic marker is used to detect the presence of the disease, being present in any stage during cancer development (Mishra & Verma 2010). Bladder tumor antigen (BTA) and nuclear matrix protein-22 (NMP-22) are examples of approved diagnostic biomarkers by the Food and Drug Administration (FDA) for bladder cancers (Lau et al. 2009). A prognostic biomarker is used to predict the course of the disease and to indicate the aggressiveness of the tumor (Gam 2012). For example, the glycoprotein CA125 is a prognostic biomarker of the ovarian cancer (Huang et al. 2010). A predictive marker is used to predict the response of a patient to specific therapeutic interventions. For instance, the predictive biomarker human epidermal growth factor receptor HER2 predicts the response to trastuzumab in breast cancer (Henry & Hayes 2012).

On the basis of biochemical molecules, cancer biomarkers include a broad range of entities, such as DNA, RNA, micro RNA, proteins, carbohydrate, lipids, and small metabolites, cytogenetic and cytokinetic parameters found in the body fluid (Bhatt et al. 2010). Proteomic markers are the most important biomarkers because they are the main executioner molecules in cells and they are more relevant to the disease state initiation and progression (Srivastava et al. 2005). Currently, the only approved biomarkers by the Food and Drug Administration (FDA) available for clinical use are protein markers (Mishra & Verma 2010). Table 1 lists some of the approved protein biomarkers by FDA in current clinical use (Ry et al. 2013). Unfortunately, in general, the available markers lack the specificity and sensitivity to be used in early detection (Gam 2012). For example, CA15.3, CA27.29, and CEA are breast cancer biomarkers recommended by the FDA but they are useful only for monitoring advanced breast cancers (Mirza et al. 2008). Therefore, researchers are working hardly in order to identify reliable cancer biomarkers that can be effectively be used for early cancer detection. Osteopontin is under study as a diagnostic and prognostic cancer biomarker. In fact, several works reported osteopontin

as an important candidate marker in human cancer (Psyrri et al. 2017; Hao et al. 2016; Ferreira et al. 2016; Nassar et al. 2015; Weber 2011; Ahmed et al. 2011). However, it has not yet been used in clinical diagnostics.

Table 2.1: List of FDA-approved protein tumor markers currently used in clinical practice (adapted from Ry et al. 2013)

Biomarker	Clinical use	Cancer type	Specimen
Pro2PSA[1]	Discriminating cancer from benign disease	Prostate	Serum
ROMA (HE4+CA-125)	Prediction of malignancy	Ovarian	Serum
OVA1 (multiple proteins)	Prediction of malignancy	Ovarian	Serum
HE4[2]	Monitoring recurrence or progression of disease	Ovarian	Serum
Fibrin/ fibrinogen degradation product (DR-70)	Monitoring progression of disease	Colorectal	Serum
AFP-L3%	Risk assessment for development of disease	Hepatocellular	Serum
Circulating Tumor Cells (EpCAM, CD45, cytokeratins 8, 18+, 19+)	Prediction of cancer progression and survival	Breast	Whole blood
p63 protein	Aid in differential diagnosis	Prostate	FFPE tissue
c-Kit	Detection of tumors, aid in selection of patients	Gastrointestinal tumors	FFPE tissue
CA[3]19-9	Monitoring disease status	Pancreatic	Serum, plasma
Estrogen receptor (ER)	Prognosis, response to therapy	Breast	FFPE tissue
Progesterone receptor (PR)	Prognosis, response to therapy	Breast	FFPE tissue
HER-2/neu	Assessment for therapy	Breast	FFPE tissue
CA-125	Monitoring disease progression, response to therapy	Ovarian	Serum, plasma
CA15-3	Monitoring disease response to therapy	Breast	Serum, plasma
CA27.29	Monitoring disease response to therapy	Breast	Serum
Free PSA[4]	Discriminating cancer from benign disease	Prostate	Serum
Thyroglobulin	Aid in monitoring	Thyroid	Serum, plasma

[1] pro-prostate specific antigen;[2] Human epididymis protein; [3] Cancer antigen;[4] prostate-specific antigen

2.3. Osteopontin: A potentially important cancer biomarker

Osteopontin (Fig. 2.1) is an acidic glycoprotein rich in arginine, glycine and aspartate in the molecular weight range of 33 to 60 kDa (Rangaswami et al. 2006; Sase et al. 2012; Ahmed et al. 2011).

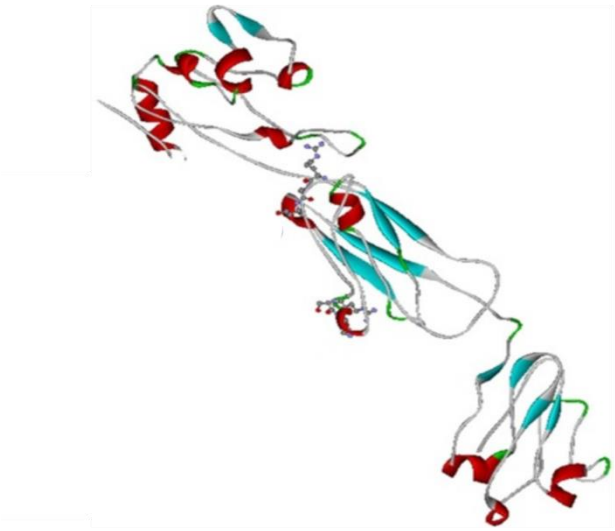

Figure 2.1: Tertiary structure of the osteopontin (Sivakumar et al. 2014)

It was first identified as a major protein in bone and subsequently found to be expressed by several tissues in the human body such as kidney, brain, macrophages, vascular smooth muscle cells and many cells of epithelial linings (Rangaswami et al. 2006). It is also overexpressed by tumor cells from multiple cancer types (Shevde & Samant 2014). In fact, clinical studies have revealed that higher expression of osteopontin is found in tumor tissue and serum of different types of cancers suggesting that osteopontin may be used as a diagnostic and prognostic biomarker for various cancers (Weber et al. 2010). Indeed, altered osteopontin levels have been associated with breast cancer (Psyrri et al. 2017; Macrì et al. 2009), thyroid cancer (Ferreira et al. 2016), colorectal Cancer (Huang et al. 2016), leukemia (Liersch et al. 2015), lung cancer (Shojaei et al. 2012), gastrointestinal stromal tumors (Hsu et al. 2010), ovarian Cancer (Huang et al. 2010), pancreatic (Collins et al. 2012) and renal cell carcinoma (Matušan-Ilijaš et al. 2011). Osteopontin acts as an important molecule that is involved in all the stages of cancer progression including tumor invasion, angiogenesis and metastasis (Ahmed et al. 2011). It acts as an important molecule at different steps of the cancer process. Briefly, high levels of osteopontin favor the survival and proliferation of cancer cells at the primary site. Osteopontin, then, bind to αvβ3 integrin and/or CD44 and activate both the matrix metalloproteinases (MMPs) and the urokinase plasminogen activator (uPA) which promote local proteolysis of the

basement membrane and enable cancer cells to detach from the primary tumor mass and invade the stroma and the surrounding tissue. The expression of osteopontin by tumor cells induce the angiogenesis by promoting the migration and adhesion of activated endothelial cells. Osteopontin acts as a chemotactic and adhesion molecule for macrophages and promotes their infiltration of the tumor. The presentation of osteopontin on the cancer cell surface enables them to sequester and activate complement factor H which protect them from the host immune system and enable them to travel and reach distant organs. At distant sites, cancer cell forms a secondary colony. Proliferative, survival and angiogenenic signals by newly formed metastatic colonies occur similarly to those that are used during the early steps of tumor progression (Kothari et al. 2016; Rangaswami et al. 2006; Rittling & Chambers 2004).

Although, osteopontin is found in all body fluids produced normally by body organs, it can be suggestive of tumor activity when detected in high amounts in the blood. For instance in hepatocellular carcinoma, the plasma osteopontin level in patients with hepatocellular carcinoma (HCC) is equal to 178 ng/ml whereas, it is equal to 37.5 ng/ml in healthy persons (Salem et al. 2013; Psyrri et al. 2017; Liang et al. 2011). Therefore, osteopontin may be envisaged as a possible non specific cancer biomarker.

2.4. Osteopontin detection

Without a doubt, the enzyme-linked immunosorbent assay (ELISA) dominates at present the field of protein detection and quantification (Li et al. 2016). Bramwell et al. (2014) used an ELISA technique to measure the osteopontin levels in plasma samples of patients with breast cancer. Generally, ELISA is a biochemical test that uses antibodies and an enzyme-mediated color change to detect the presence of an antigen like proteins, hormones, peptides, etc. or antibody in a given sample (Gan & Patel 2013). Despite its widespread use, some limitations have to be considered. In fact, nonspecific binding of the antibody or antigen to the plate will lead to a falsely high-positive result. In addition ELISA cannot distinguish between antigenically identical analytes. For instance the same ELISA assay will often recognize many or all different isoforms of the same protein in a sample. Moreover, the assay requires some specialized equipment, like a spectrophotometric microplate reader, large amounts of sample and skilled technicians (Chatziharalambous et al. 2016; Li et al. 2016). Therefore, it is urgent to develop new

detection techniques for protein cancer biomarkers that circumvent the above mentioned limitations of conventional ELISA.

2.5. Biosensor: a promising alternative for osteopontin detection

Biosensors are powerful analytical devices that consist of a bioreceptor compound such as an antibody or nucleic acid immobilized on a transducer surface, which is capable of providing a signal due to the interaction between the bioreceptor and the analyte (Vigneshvar et al. 2016). Biosensors are able to detect a wide range of analytes in complex matrices and have been applied in many fields such as food industry, medical field and environmental monitoring. They provide better stability and sensitivity as compared with the conventional methods such as enzyme-linked immunosorbent assays, 2-D western blotting, and 2-D gel electrophoresis (Kraatz & Amini 2015; Mehrotra 2016). The main components of biosensors are:

- The bioreceptors (biorecognition elements) which could specifically recognize and identify target (Han et al. 2010).
- Signal transducer, which could transform the biological signal into an electrical signal with high sensitivity and minimum disturbance to the measured analyte.
- A display which transforms the measured electrical/optical signal into a digital format for end users (Cheng et al. 2009; Han et al. 2010).

The existing biosensors can be classified into immunosensors, enzymosensors, aptasensors, etc. based on the nature of the bioreceptor such as antibodies, enzymes and aptamers respectively (Mehrotra 2016).

2.6. Aptasensor: a class of biosensor

An aptasensor is a particular class of biosensor where the biological recognition element is a DNA or RNA aptamer. In an aptasensor, the aptamer recognizes the molecular target towards which it was previously selected in vitro (Duan et al. 2016). Aptamers refer to artificial nucleic acids DNA or RNA generated from combinatorial libraries of oligonucleotides that undergo a selection methodology to bind with high affinity and specificity to analytes of interest. This selection methodology is termed SELEX (systematic evolution of ligands by exponential enrichment) (Cheng et al. 2009). Detailed reviews of the SELEX process can be found in the literature (Ozer et al. 2014; Stoltenburg et al. 2007). Compared to other existing biological recognition elements,

aptamers exhibit several advantages in terms of stability, design flexibility, and cost-effectiveness. To name a few, stability to long-term storage and under a wide range of buffer conditions, easy synthesis, resistance to denaturation and degradation, reversible thermal denaturation and ability to bind to targets with selectivity, specificity, and affinity, equal and often superior to those of monoclonal antibodies (Lowe 2008; Meirinho et al. 2015; Moreno 2014).

2.7. Dual-aptasensor array

A dual-aptasensor array is an aptasensor composed of two different immobilized aptamers which are able to bind independently with the same or different targets that are present in the sample (Khang et al. 2017). An aptasensor dual-array offers higher specificity compared with the uniplexed format (Cao et al. 2017; Song et al. 2014). It is expected that aptamer array based technology will become a powerful diagnostic tool. In fact, the biotechnology company SomaLogic has developed different enhanced aptamer arrays for the discovery of potential biomarkers and has demonstrated their successful use (Gold et al. 2010). One of the already available commercial versions of aptamer arrays is SOMAscan™ which allows the simultaneous precise measurement of over 1000 proteins (Webber et al. 2014).

Whenever developing a dual-aptasensor array, relevant factors must be considered such as the detection technique, the electrode/transducer surface and the immobilization method of the bioreceptor. The following section will describe in detail these factors.

2.7.1. Detection technique

To transform the bioreceptor-target reaction into a detectable signal, several transducer technologies can be used. The existing transducers can be classified into electrochemical, optical, acoustical, piezoelectric, calorimetric, magnetic and micromechanical based on the property to be determined such as electricity; light; sound; mass change; heat; magnetism; and viscosity, and pressure respectively (Newman & Turner 2007). The most frequently cited in the literature and most common are electrochemical aptasensor arrays that hold a leading position among the presently available sensors. Indeed, they offer an extensive range of advantages over other existing transducers such as low cost, remarkable detection limits, experimental simplicity, capability to work with turbid samples, fast response, multi-target detection, and easy

miniaturization (Meirinho et al. 2015; Arya et al. 2007). Electrochemical methods are generally based on electrochemical processes taking place at an electrode surface. These electrochemical processes involve loss of electrons (oxidation) or gain of electrons (reduction) that a material undergoes during a redox reaction. These reduction and oxidation reactions can be used to evaluate the concentration of chemical species in solutions, its kinetics, reaction mechanisms, and chemical status. A standard potential E^0 exists for each redox couple at which the reduced and oxidized forms are present at equal concentrations. As a result of an imposed potential on the working electrode with respect to the reference electrode (for example, by the use of a potentiostat), the redox couples present at the electrode respond to this change and adjust their concentration ratios according to the following Nernst's equation (2.1):

$$E = E^0 + \frac{RT}{NF} \ln \frac{[ox]}{[red]} \tag{2.1}$$

where, E^0 is standard potential, F is Faraday's constant, T is absolute temperature, and [ox] and [red] are concentrations of oxidation and reduction centers respectively (Arya et al. 2007).

In order to study and understand the electrochemical processes, voltammetric, amperometric, potentiometric, impedimetric and conductometric techniques are used to measure parameters such as current and potential, current, potential, impedance, and conductance, respectively (Meirinho et al. 2015). The measurement of current resulting from the application of a potential is known as voltammetry. During voltammetric measurements, accurate application of potential functions and the measurement of the resultant current are ensured by three electrodes (working, auxiliary or counter, and reference electrodes; WE, AE or CE, and RE, respectively) along with the potentiostat instrument.

The resulting plot of the current versus applied potential, called voltammogram, provides quantitative and qualitative information about the species involved in the oxidation or reduction reaction. Voltammetric techniques possess several analytical advantages which include low related observed noise, excellent sensitivity, possibility of multiple detection, very large useful linear concentration range for species (10^{-12} to 10^{-1} M), large number of useful solvents and electrolytes, a wide range of temperatures and rapid analysis times (Mendoza et al. 2015).

Different potential function can be applied to the WE to drive the reaction and several materials can be used as the working electrode. (Arya et al. 2007). The different voltammetric techniques are distinguished from each other primarily by the different modes of the potential application. One of these voltammetric techniques is cyclic voltammetry (CV) which is a useful and versatile electroanalytical technique for the study of electroactive species. In CV, a potential is applied and the resulting current intensity is measured in an electrolytic solution. As the applied potential reaches the oxidation potential of the analyte, the current will increase and then falls off when the concentration of the analyte is reduced close to the electrode surface. Then, the applied potential is reversed and reach a potential at which the reduction of product formed, during forward scan, starts and produces a current of reverse polarity from the forward scan. The reduction and oxidation peaks usually have a similar shape (Fig. 2.2). Anodic peak potential Epa, cathodic peak potential Epc, anodic peak current *I*pa and cathodic peak current *I*pc are the measured parameters in CV (Sethi 1994; Farghaly et al. 2014). CV is a simple, rapid and sensitive techniques that gives reproducible results and offer the possibility to observe the oxidation peak and the reduction peak simultaneously which is quite helpful in the investigation of electrolytic processes. For instance, the evaluation of the electrode surface such as its stability and purity, the cleaning of the electrode surface, the immobilization of the bioreceptor on the electrode surface and the detection of the formed complex bioreceptor-target (Sethi 1994; Meirinho et al. 2015).

Another voltammetric technique is square wave voltammetry (SWV) (Fig. 2.3) which is much more sensitive than CV due to the elimination of the background current during the experiment (Ferreira et al. 2011). The major advantage of SWV beside the higher sensitivity is its speed. In fact SWV allows a very fast analysis (few seconds) (Farghaly et al. 2014; Dias et al. 2017).

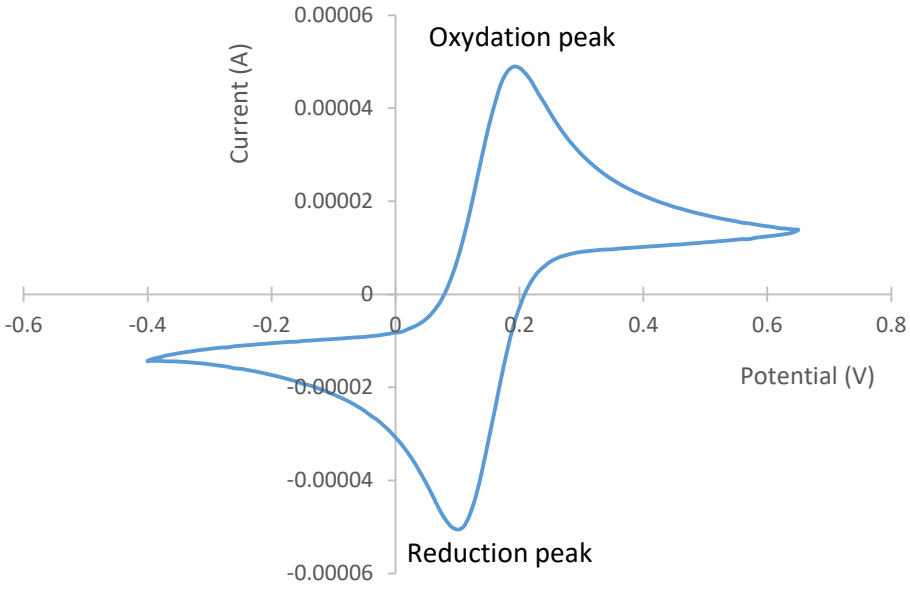

Figure 2.2: Cyclic voltammogram

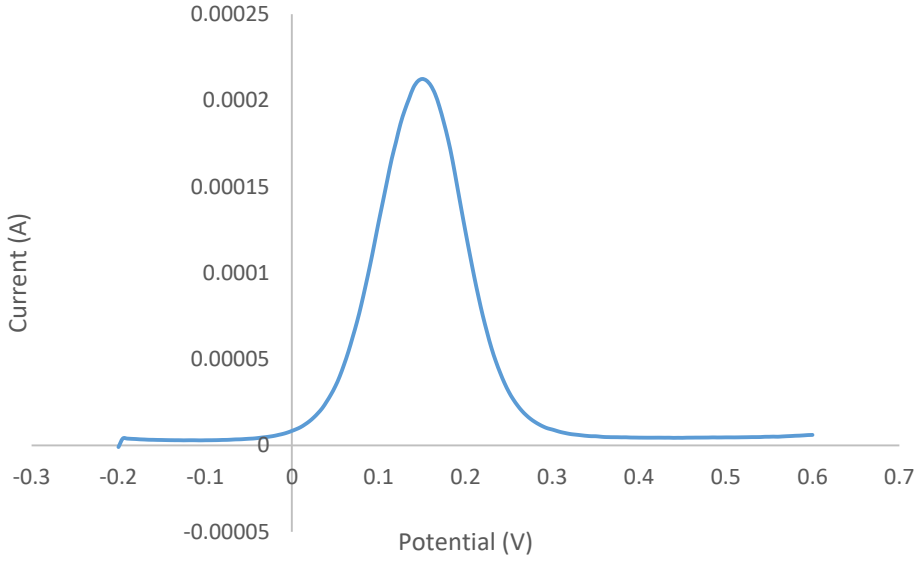

Figure 2.3: Square-wave voltammogram

The height of the peak is proportional to the concentration of the electroactive species. SWV allows detection limits as low as 10^{-8}M (Mendoza et al. 2015). Other voltammetric techniques include Normal Pulse Voltammetry (NPV), Differential Pulse Voltammetry (DPV), Polarography, Anodic Stripping Voltammetry, Cathodic Stripping Voltammetry and Adsorptive Stripping Voltammetry (Mendoza et al. 2015).

2.7.2. Immobilization of Aptamers

The aptamers immobilization into an electrode surface is a crucial step in electrochemical aptasensors development. Many available strategies allow reliable immobilization of aptamers so that they retain their biophysical characteristics and binding abilities and minimize nonspecific binding event (Radi & Abd-Elgawad 2011). The choice of a suitable immobilization strategy is determined by the physicochemical properties of both surface and aptamers. Aptamers can be physically adsorbed on the surface, covalently attached with functional groups or immobilized by streptavidin-biotin interaction (Rhouati et al. 2016). Physical adsorption does not require any aptamer modification. It is based on ionic interactions occurring between the negatively charged groups of the aptamers and positive charges covering the surface. Although it is a fast and simple method, the resulting immobilized aptamers are randomly oriented on the surface and desorption can occur by detergent, change of pH or ionic strength (Nimse et al. 2014). Covalent attachment methods allow good stability of aptamers and high binding strength interactions. They are based on interactions between the surface functional groups, such as thiol and amines, and aptamer's chemical groups. For covalent binding of biomolecules on gold surfaces, thiol-metal interactions are frequently used The thiol groups demonstrate strong affinity towards the noble metal surfaces allowing the formation of covalent bonds between the sulfur and gold atoms (Rhouati et al. 2016). In the immobilization by streptavidin-biotin interactions, streptavidin is first linked to the solid surface then the biotinylated aptamers form the complex streptavidin-biotin. Streptavidin is a tetrameric protein that has four identical binding sites for biotin, which is a small molecule, binds with a very high affinity to the streptavidin binding sites (Nimse et al. 2014).

2.7.3. Electrode surface materials

Different materials are available for the preparation of surfaces for biosensing applications. They need to fulfill, depending on the measurement technique, special requirements, such as electrical conductivity for electrochemical techniques. The most common are gold, microporous gold, graphite, glass carbon and indium tin oxide. Conducting polymers are another class of materials used for fabricating electrochemical biosensors. These include polyaniline, polypyrrole and polystyrene, which can be coated onto other sensor substrates usually gold surfaces. This leads to stable surfaces with easy handling and excellent redox recyclability (Grieshaber et al. 2008). In the last two decades

or so, screen-printing technology has been exploited in biosensors, paving the way for the development of a new range of electrode systems. Screen printed electrodes (SPE) usually include a three electrode configuration (WE, AE and RE) printed on several kinds of plastic or ceramic substrates. This configuration has given SPE an unrivaled power of adaptability and excellent accuracy.

In recent years, SPE have been extensively employed for developing novel electrochemical sensing platforms and improving their performances. This is due to the multiple advantages that SPE can offer namely, the reduction of sample volume required to as low as few microliters, and the possibility of connecting it to portable instrumentation. In addition, SPEs avoid some of the common problems of classical electrodes, such as tedious and time-consuming cleaning processes (Taleat et al. 2014). Stencils, ink and a squeeze blade are typically used in screen-printing technology. Silver ink and carbon ink are the most commonly used during the printing process of SPEs (Yamanaka et al. 2016). Silver ink is printed as a conductive track, whereas graphite ink is used for the WEs; other materials such as gold, platinum and silver based inks are also used. Carbon inks which consist of graphite particles, polymeric binder and other additives are a widespread material because they are relatively cheap, easy to modify and chemically inert. Gold ink pastes are less employed than carbon because of their higher cost (Taleat et al. 2014). However, the affinity between thiol moieties and gold allows SPEs with gold WEs to be easily modified with the formation of self-assembled monolayers (SAMs), creating a significantly increased interest for gold SPEs to be employed in electrochemical biosensors (Yamanaka et al. 2016). The SAMs are used for the immobilization of biological recognition elements on the electrode surface. For instance, carboxyl groups serve for antibody immobilization, esters for amine couplings and biotin can be used to bind streptavidin and further biotin functionalized biomolecules. It is important, in electrochemical applications, that the SAM allows electron and analyte diffusion (Grieshaber et al. 2008). Some materials, such as, gold, silver, platinum, palladium, other metal nanoparticles and carbon nanotubes and graphene based inks allow enhanced immobilization efficiency of biological molecules and accelerate the electron transfer rate on electrode surface (Taleat et al. 2014).

It is of utmost importance that, after selecting the electrode surface material, the immobilization method and the detection technique, the experimental conditions regarding the immobilization steps (namely, concentration, time and temperature) should

be optimized and for that experimental design strategies may be used to reduce the number of assays and to really establish the best conditions taking into account the possible effects of each individual parameters but also the synergetic effect of the interactions between parameters.

2.8. The two-level factorial design (2^k factorial design)

Factorial designs are statistical multivariate techniques that include a series of experiments that are designed to evaluate the possible effect of two or more factors, each with discrete possible levels, where all possible combinations of the levels of the factors are investigated (Aghahosseini et al. 2013). They are widely used in experiments involving several factors where it is necessary to study the joint effect of the factors on a response. The effect of a factor is defined to be the change in response produced by a change in the level of the factor. This is called a main effect because it refers to the primary factors of interest in the experiment. If there is an interaction between the factors, the difference in response between the levels of one factor is not the same at all levels of the other factors (Montgomery 2008).

In research work, special cases of the factorial design are widely used. The most common of these special cases is the two-level factorial design (2^k factorial design) in which k factors are studied simultaneously each one at only two levels. The 2^k design provides the smallest number of runs with which k factors can be studied in a complete factorial design. In fact, with three factors, the factorial design requires only 8 runs versus 16 for an one-factor-at-a-time (OFAT) experiment with equivalent power. The advantage of factorial design becomes more pronounced as more factors are added (Anderson. 2000). In 2^k factorial design, the factors with their levels should be fixed, the designs are completely randomized, the usual normality assumptions are satisfied and the response is assumed to be linear over the range of the factor levels chosen because there are only two levels for each factor (Montgomery 2008).

To check for the accuracy of the fitness, center points are usually incorporated in the factorial structure. Center points are created by setting all factors at their midpoint between their low and high levels. The center point should be replicated to provide more power for the analysis. These points, along with all the others, must be performed in random order. The center points act as a barometer of the variability in the system. The average response value from the actual center points is compared to the estimated value

that comes from averaging all factorial points. If the actual center point value are higher or lower than predicted by the factorial design points, there is curvature of the response surface in the region of the design (AlcheikhHamdon et al. 2015; Anderson. 2000).

CHAPTER 3

Materials and methods

3.1. Materials

3.1.1. Reagents and solutions

Diethypyrocarbonate (DEPC), 3,3'-dithiodipropionic acid (DPA), N-(3-dimethylaminopropyl)-N-ethylcarbodiimide hydrochloride (EDC), N-hydroxysuccinimide (NHS), ethanolamine (ETA) and sulfuric acid (purity of 99.999%) were purchased from Sigma-Aldrich. Potassium hexacyanoferrate (III) ($K_3Fe(CN)_6$) and potassium hexacyanoferrate (II) ($K_4Fe(CN)_6$) were acquired from Acros Organics and potassium dihydrogen phosphate (KH_2PO_4) from Merck. Sodium chloride (NaCl), potassium chloride (KCl) and sodium hydrogen phosphate (Na_2HPO_4) were obtained from Panreac. Lyophilized recombinant human osteopontin was purchased from R&D systems and manipulated according to the manufacturers' specifications.

The RNA aptamer and DNA aptamer were synthesized by Integrated DNA Technologies (Belgium), their sequences were as follow: RNA aptamer (5'-Biotin- CGG CCA CAG AAU GAA AAA CCU CAU CGA UGU UGC AUA GUU G-3') and DNA aptamer (5'-Biotin-TGT GTG CGG CAC TCC AGT CTG TTA CGC CGC-3') (Meirinho 2016). Phosphate buffer saline (PBS) solution (137 mM NaCl, 2.7 mM KCl, 8.1 mM Na_2HPO_4 and 1.47 mM KH_2PO_4) with an adjusted pH of 7.4 was used to prepare the ferro/ferricyanide redox probe, dilute the working solutions if needed and wash the electrodes. The ferro/ferricyanide redox probe (5 mM $K_3Fe(CN)_6$ and $K_4Fe(CN)_6$ (1:1) and 10 mM KCl in 100 mL of PBS), with an adjusted pH of 7.4, was prepared. Stock solutions of 200 mM EDC, 100 mM NHS, as well as the stock solution of 1 mg/ml of septravidin in PBS (pH 7.4) were stored at -20 ºC before use. Stock solutions of 200 nM DPA and 100 mM of ETA were stored at 4 ºC. Stock solution of osteopontin was prepared according to the manufacturer specifications and was stored at -20 ºC. The osteopontin working solution was obtained by dilution of the stock solutions with PBS buffer and was stored at 4 ºC until use. Deionized water (18.2 MΩ) purified by a milli-QTM system (Millipore) was used was to rinse the electrode surface and for aqueous solutions preparation. Stock solutions of DNA and RNA aptamers were prepared with ultra-pure water containing 1% DEPC (v/v) to avoid the RNase interference at 100 μM. The working DNA and RNA aptamer solutions were prepared by dilution of the stock solutions using PBS.

3.1.2. Apparatus

The (Dual-SPGE) were purchased from DropSens (Oviedo, Spain). They include a four-electrode system configuration (two WEs, RE and AE) printed on the same strip of ceramic substrate (3.4 x 1.0 x 0.05 cm) and were subjected to low temperature (BT) curing ink. They are composed of two ellipses of gold-BT WEs (with a surface of 6.3 mm^2 each) arranged in a parallel way in the ceramic strip, an Ag/AgCl RE and a gold-BT CE (19.8 mm^2 and 1 mm wide) (Fig. 3.1). A Potentiostat-Galvanostat device (PG580, Uniscan Instruments) was used to record CV and SWV signal profiles (Fig. 3.2).

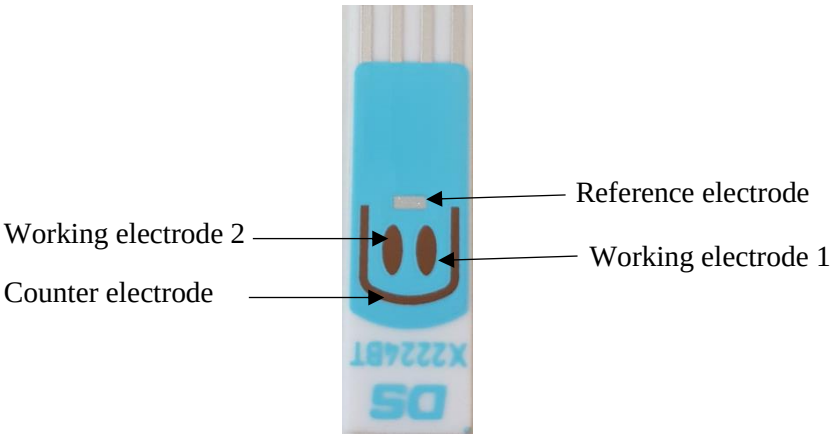

Figure 3.1: Dual-screen-printed gold electrode (Dual-SPGE)

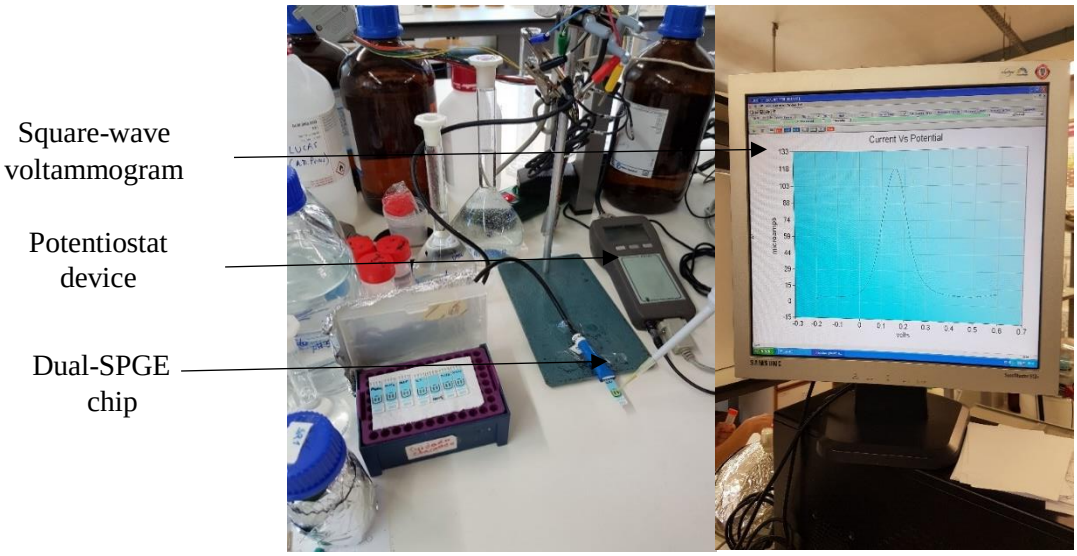

Figure 3.2: Electrochemical measurements by the Potentiostat-Galvanostat device

3.1.3. Software

Two statistical software, Design-Expert and Statistical Package for Social Sciences (SPSS), were used for the experimental design and regression analysis of the experimental data. The UiEChem™ software was used to study the electrochemical processes taking place at the electrodes surfaces.

3.2. Methodology

3.2.1. Cleaning and homogenization of the working electrodes

The gold surface of the electrode is subjected to ambient contaminants affecting electrochemical measurements. In fact, the peak currents in CV and SWV depend on the homogeneity and composition of the gold electrode surface (Fischer et al. 2009). For this reason, the gold electrode surface must be cleaned before it is chemically modified for the immobilization step.

The electrode was electrochemically cleaned by successively cycling the electrode using three weak sulfuric acid solutions (H_2SO_4 (0.5 M), KCl (0.01 M)/ H_2SO_4 (0.1 M) and H_2SO_4 (0.05 M)), under a potential range between -0.3 and +1.5 V at a scan rate of 100 mV/s. The cleaning procedure ended when a representative cyclic voltammogram of a clean gold electrode was obtained.

In order to ensure the uniformity of the WE, $[Fe(CN)_6]^{-3/-4}$ solution was used to verify if the typical CV or SWV voltammogram of an homogenized gold electrode was reached.

3.2.2. Functionalization of the working electrodes

The procedure followed to functionalize the WE was previously described in Meirinho et al. (2015). The electrode surface must be chemically modified to ensure an efficient immobilization of the aptamers. For that, the WE was incubated with DPA during 30 min at room temperature in order to form the self-assembled monolayer (SAM) then rinsed with deionized water. To facilitate the binding with the amino group of the streptavidin, the carboxylic groups of the SAM were activated with EDC and NHS (1:1 v/v) during 60 min at room, the electrode is then rinsed with deionized water .After that, the WE surface was incubated with streptavidin solution overnight at 4 ºC to enable the binding of the amine groups with the activated carboxylic groups of the self assembled monolayer. To block any remaining activated carboxyl groups, the WE surface was

exposed to ETA during 20 min at room temperature. Finally, the electrode was rinsed with PBS buffer.

3.2.3. Immobilization of the DNA and RNA aptamers

After the functionalization step, the WE is ready for the aptamers immobilization. The biotinylated RNA and DNA aptamer solutions were prepared by dilution to the desired concentration using PBS buffer. Three different concentrations were studied namely, 0.5µM, 1µM and 1.5µM. The pretreatment of the aptamers solution is an essential step that allows the formation of a flexible aptamer structure that can interact easily with the streptavidin on the WE surface. This step consists in exposing the aptamers solution to heat treatment (95 ºC during 5 min, 4 ºC for 5 min and 10 min at room temperature). After the heat treatment, the biotinylated aptamer was attached to the modified gold surface through the streptavidin–biotin interaction. Different aptamers' immobilization times (20 minutes, 40 minutes and 60 minutes) and different incubation temperatures (4°C, 24°C and 44°C) were evaluated (as described in Tables 3.1 to 3.3). The electrode was then rinsed with PBS buffer to remove the unbound aptamers.

3.2.4. Electrochemical measurements

After the aptamers immobilization, 100 µl of $[Fe(CN)_6]^{3-/4-}$ solution (5 mM $K_3Fe(CN)_6$ and $K_4Fe(CN)_6$ (1:1) and 10 mM KCl in 100 mL of PBS) was dropped into the chip covering the four electrodes (two WEs, RE and AE) . The electrochemical analysis was, then, performed at room temperature using CV (under a potential range between -0.4 and 0.65 V at a scan rate of 0.05 V/s) and SWV (under a potential range between -0.2 and 0.6 V at a frequency of 25 Hz and a pulse height of 0.025 V). For both techniques, the obtained current peak I_0 was recorded.

3.2.5. Osteopontin incubation

Osteopontin solution (200.2 nM) was prepared by solubilizing the lyophilized osteopontin in PBS buffer. 2.5 µl of this solution was dropped on each WE and kept at different incubation temperatures (4°C, 24°C or 44°C) for 30, 60 or 90 minutes (Tables 3.1 to 3.3). Then the electrode surface was washed with PBS buffer to remove the unbound proteins.

3.2.6. Calculation of the current peak decrease

After osteopontin incubation, the electrochemical analyses were done as those performed after aptamers immobilization and the obtained current peak I_1 was recorded. For both CV and SWV techniques, the relative current change was calculated according to the equation (3.1):

$$\Delta I = (I_0 - I_1)/I_0 \times 100 \quad (3.1)$$

where, ΔI is the relative current change (%), I_0 and I_1 represents the peak current (mA) before and after the sample incubation, respectively. Four signal responses were obtained namely ΔI_{SWV}^{DNA} , ΔI_{SWV}^{RNA} , ΔI_{CV}^{DNA} and ΔI_{CV}^{RNA} which correspond to the relative current change when using SWV as electrochemical technique and DNA as aptamer, relative current change when using SWV as electrochemical technique and RNA as aptamer, relative current change when using CV as electrochemical technique and DNA as aptamer, and relative current change when using CV as electrochemical technique and RNA as aptamer, respectively

3. Optimization of the experimental conditions

The performance of the developed dual-aptasensor array can be severely affected by the experimental conditions (Meirinho 2016). As previously reported, a 2^k factorial experimental design was employed in order to find the key factors responsible for a significant effect on the electrochemical response of the dual-aptasensor, aiming to maximize its response. This technique was used to reduce the number of experiments, time, overall process cost and to get a better overall perception of the single and simultaneous effects of the parameters under study (Elhalil et al. 2016).

Fig. 3.3 illustrates the steps taken for the establishment and the analysis of the two-level factorial design. Steps 3, 5, 6, 7, 9, 10 and 12 were done using the Design-Expert® software. Relevant factors which may affect the aptasensor response were studied. Four factors were chosen, namely, (X_1) aptamer concentration, (X_2) time of aptamer immobilization into dual-screen printed gold electrodes (Dual-SPGE), (X_3) the aptamer-protein interaction time and (X_4) incubation temperature (step 1 in Fig. 3.3). Both factors, aptamer concentration and time of aptamer immobilization into dual-screen printed gold electrodes (Dual-SPGE), can affect the coverage of the electrode surface with aptamers.

The time of aptamer-protein interaction can have an influence on the formation of the aptamers-protein complex. The incubation temperature may alter the spatial configuration of the aptamer and/or the osteopontin.

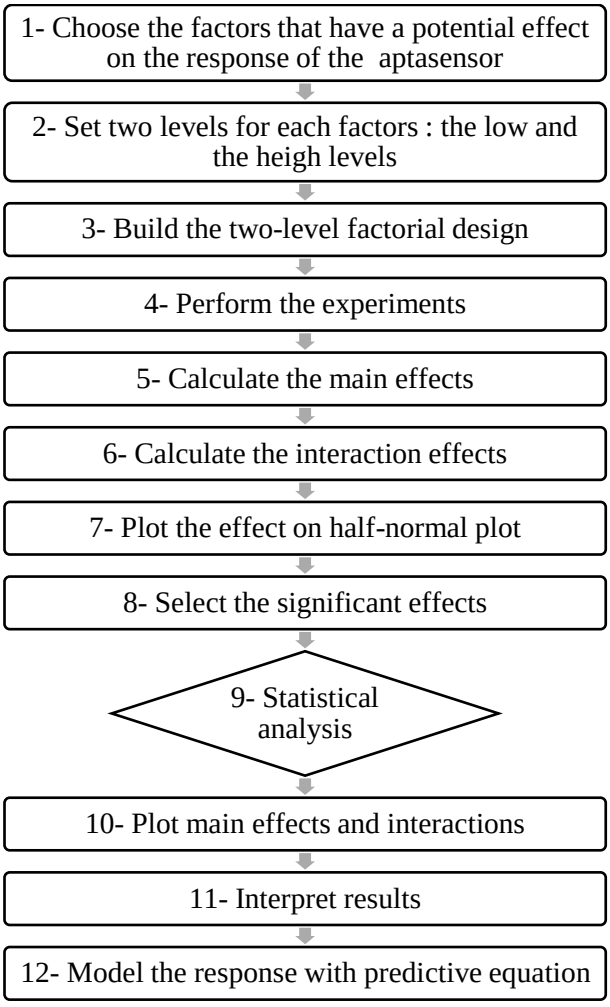

Figure 3.3: Steps of creation and analysis of the 2^k factorial design

Table 3.1: Factors and levels for 2^k factorial design

Real factors	Coded factors (X_i)	Units	Low level (-)	High level (+)
Aptamer concentration	X_1	µM	0.5	1.5
Time of aptamer immobilization into dual-screen printed gold electrodes (Dual-SPGE)	X_2	min	20	60
Aptamer-protein interaction time	X_3	min	30	90
Incubation temperature	X_4	°C	4	44

The four chosen factors, X_1, X_2, X_3 and X_4, are all numerical so they can be adjusted to any level. Each studied factor was adjusted to two levels, a low (-) and a high (+) level (step 2 in Fig. 3.3). A general rule is to set levels as far apart as possible so it will be more likely to see an effect, but not exceed the operating boundaries (table 3.1).

Once the factors and their levels were set, the 2^k factorial design was built by the Design-Expert® software (step 3 in Fig. 3.3). Because we have four factors, each with two levels, the 2^k factorial design produces 16 runs ($2^4 = 16$). Center points were included into the design in triplicate to check for the assumption of linearity in the factor effects, in other words, to detect an eventual presence of curvature.

If the curvature is not significant, the relationship between the aptasensor response (the current change) and the chosen factors fits a first-order model (the model will be explained in more details in the twelfth step). If the curvature is significant, a second-order model is more appropriate. Center points are created by setting all factors at their midpoints, they correspond to the zero level (table 3.2).

Table 3.2: Two-level factorial with center points

Coded factors (X_i)	Units	Low level (-)	Center (0)	High level (+)
X_1	µM	0.5	1	1.5
X_2	min	20	40	60
X_3	min	30	60	90
X_4	°C	4	24	44

The final generated 2^k factorial design, taking into account the three replicates of the center points, produces 19 runs. Experiments were conducted as shown in table 3.3 which is generated by the Design-Expert® software (step 4 in Fig. 3.3). The run order of the design was completely randomized to offset any lurking variables. Four responses of the 19 runs were recorded and the relative current changes (ΔI_{SWV}^{DNA}, ΔI_{SWV}^{RNA}, ΔI_{CV}^{DNA} and ΔI_{CV}^{RNA}) were determined using equation 3.1.

The average effect of a factor in a two-level factorial design is defined as the change in response produced by a change in the level of that factor averaged over the levels of the other factor (Montgomery 2008).

Table 3.3: 2^k factorial design in randomized standard order created by Design-Expert® software

std	run	X_1	X_2	X_3	X_4
10	1	+	-	-	+
1	2	-	-	-	-
11	3	-	-	+	+
9	4	-	-	-	+
8	5	+	+	+	-
18	6	0	0	0	0
7	7	-	+	+	-
5	8	-	+	-	-
15	9	-	+	+	+
19	10	0	0	0	0
12	11	+	-	+	+
3	12	-	-	+	-
13	13	-	+	-	+
2	14	+	-	-	-
14	15	+	+	-	+
6	16	+	+	-	-
16	17	+	+	+	+
4	18	+	-	+	-
17	19	0	0	0	0

Main effects of each of the chosen factors (X_1, X_2, X_3 and X_4) were calculated as follows (step 4 in Fig. 3.3):

$$Effect = \sum_{8} \Delta I_{+} - \sum_{8} \Delta I_{-} \quad (3.2)$$

Where ΔI_{+} refers to the aptasensor response when the factor is set at the high level and ΔI_{-} refers to the aptasensor response when the factor is set at the low level.

The full-factorial design allows estimation of all six two-factor interactions (X_1 X_2, X_1 X_3, X_1 X_4, X_2 X_3, X_2 X_4, and X_3 X_4), all four three-factor interactions (X_1 X_2 X_3, X_1 X_2 X_4, X_1 X_3 X_4 and X_2 X_3 X_4) , as well as the four-factor interaction (X_1 X_2 X_3 X_4). The signs of interaction effects is determined by multiplying the signs of parent terms. The interaction effects are then calculated using the general formula shown previously (equation 3.2) (step 6 in Fig. 3.3). After calculating the effects related to the main and interaction effects, their statistical significance was evaluated aiming to verify if their

contribution was due to normal variations in the aptasensor response (noise) or not. Plotting the absolute value of all effects on a half-normal probability plot, separates the effects into large, repeatable effects and the small, likely to be noise effect. The half-normal plot of effects makes it very easy to see at a glance what is significant (step 7 in Fig. 3.3). In the half-normal probability plot, the not statistical significan effects would be located on a line near zero whereas the significant effects are off the line. The latter are selected in order to establish the model and study the effects of the factors and their interactions (step 8 in Fig. 3.3). Effects with no significance can be included to keep a hierarchical model. The significance of the model was evaluated (step 9 in Fig. 3.3) using analysis of variance (ANOVA). A model having a p-value lower than 0.05 is considered significant. In the same way, the main and interaction effects of each factor which have p-value <0.05 are significant. The fit of the model was further statistically checked by the coefficient of determination R^2 and the predicted coefficient of determination (R^2 or Q^2 predicted). The R^2 value is always between 0 and 1. The closer the R^2 value is to 1, the better the model predicts the response. It gives an idea of how well current runs can be reproduced by the model (Elhalil et al. 2016; Neta et al. 2011). R^2 value higher than 0.75 indicates that the model is good.

The Q^2 value informs about the goodness of prediction, indicating how well new experiments can be predicted using the model. A Q^2 value higher than 0.60 indicates that the model is good. The discrimination ability of the model was also assessed by measuring the adequate precision value, which compares the response to the noise ratio. A value greater than 4 is envisaged to assure adequate model discrimination (Dominguez et al. 2012).

If the model created is not significant or the R^2 value is lower than 0.75 or the Q^2 value is lower than 0.25 or the adequate precision value is lower than 4, a new model terms from the half-normal probability plot should be selected and new model should be created.

If the statistical analyses do not reveal any problem in the model, we plot and interpret interactions. The interaction graphs show lines bracketed by least significant difference (LSD) bars at either end. If the LSD bars do not intersect or overlap, this means that the effects are significantly different.

In a 2^k factorial design, it is easy to express the results of the experiment in terms of a predictive equation (step 11 in Fig. 3.3). The following equation (equation 3.3) represents the model used to predict the response of the dual-aptasensor array:

$$\Delta I = \beta_0 + \sum_{i=1}^{4} \beta_i X_i + \sum_{i<j}^{6} \beta_{ij} X_i X_j + \sum_{i<j<k}^{3} \beta_{ijk} X_i X_j X_k + \beta_{1234} X_1 X_2 X_3 X_4 \quad (3.3)$$

Where ΔI is the predicted response (the relative current change in percentage); the β's are parameters whose values are to be determined using the linear regression model, being β_0 the intercept, β_i and β_j the linear coefficients and $\beta_{ij,}$ β_{ijk} and β_{1234} the interaction coefficients and X_1, X_2, X_3 and X_4 are the coded factors (Dominguez et al. 2012).

CHAPTER 4

Results and discussion

Electrochemical aptasensors have been attracting a great attention in several fields such as, clinical diagnosis, environmental monitoring and food analysis, mainly due to their high sensitivity, rapid response and low-cost measurement systems (Cao et al. 2017). The performance of the developed electrochemical dual-aptasensor array for osteopontin detection is affected by several experimental conditions such as incubation temperature, the concentration of aptamers, immobilization time of aptamers and contact time between aptamers and proteins. Consequently, as several factors are involved, finding the optimal experimental conditions that allow enhancing the performance of a dual-aptasensor array can be very laborious if no alternative approaches, such as experimental design and optimization tools, are used. In the aim of minimizing time-effort and optimizing all the affecting parameters simultaneously, a 2^k factorial design was conducted with four factors (X_1) aptamer concentration, (X_2) time of aptamer immobilization into dual-screen printed gold electrodes (Dual-SPGE), (X_3) the aptamer-protein interaction time and (X_4) incubation temperature. An experimental design summary which includes design, factors and their levels, and response information are given in table 4.1.

Table 4.1 Experimental design and results obtained using the 2^4 factorial design used for the optimization of the experimental conditions of the dual-aptasensor array

Run	Coded factors				ΔI (%)[a] RNA aptamer			ΔI (%) DNA aptamer		
	X_1	X_2	X_3	X_4	SWV[b]	CV[c] (ox)[d]	CV (red)[e]	SWV	CV (ox)	CV (red)
1	+	-	-	+	10.83	7.80	11.18	12.29	16.00	13.35
2	-	-	-	-	40.93	21.58	28.74	53.86	32.26	36.91
3	-	-	+	+	38.26	9.21	9.60	44.55	9.60	12.78
4	-	-	-	+	36.78	10.42	11.13	26.68	28.74	8.10
5	+	+	+	-	37.28	13.38	14.13	48.53	19.44	19.37
6	0	0	0	0	28.02	10.84	7.94	37.02	12.40	11.28
7	-	+	+	-	34.76	14.57	16.95	35.47	11.18	15.94
8	-	+	-	-	48.98	20.39	22.62	45.88	19.43	19.67
9	-	+	+	+	25.91	13.10	20.16	40.79	22.62	21.33
10	0	0	0	0	32.41	10.78	10.66	32.78	18.69	9.33

Table 4.1 (continued)

11	+	-	+	+	0.00	0.00	2.35	29.09	7.94	11.72
12	-	-	+	-	39.09	16.94	21.06	35.70	14.13	17.74
13	-	+	-	+	46.65	15.45	19.43	50.64	11.13	17.44
14	+	-	-	-	39.13	10.99	18.69	48.40	2.35	20.82
15	+	+	-	+	45.64	17.03	19.44	43.76	14.06	19.32
16	+	+	-	-	26.51	7.58	12.40	35.96	20.16	15.53
17	+	+	+	+	38.58	11.78	14.06	47.74	21.06	17.73
18	+	-	+	-	37.67	15.60	16.00	33.26	15.16	16.81
19	0	0	0	0	35.01	15.18	15.16	32.00	16.95	13.01

[a] relative current change of the aptasensor; [b] square wave voltammetry; [c] cyclic voltammetry; [d]oxidation; [e] reduction

4.1. Effect of the experimental conditions on the response of the developed dual-aptasensor array

For both SWV and CV techniques, the response of the dual-aptasensor array was determined by measuring the current change before and after osteopontin incubation according to the equation 3.1. Under the experimental conditions of the run 2 (4°C, 0.5 µM of aptamer concentration, 20 min of aptamer incubation and 30 min of aptamer-osteopontin interaction) (Table 4.1), the peak current of SWV before osteopontin incubation for both DNA and RNA aptamer is equal to 52.2 µA and 40.9 µA respectively while it decreases to 24.0 µA and 24.1 µA respectively after protein incubation which correspond to a current decrease of 54% and 41%, respectively (Fig. 4.1 (a) and (b)). Under the same experimental conditions, the peak of CV also decreases after osteopontin incubation for both DNA and RNA aptamer from 43.7 µA and 41.7 µA to 26.9 µA and 32.7 µA, respectively, which correspond to a current decrease of 32% and 22% respectively. The drop in the intensity of the current can be explained by an inhibition of the electron transfer after the osteopontin incubation. In fact, in the absence of osteopontin, the aptamer, which is immobilized into the gold surface of the WE, showed a dynamic state and flexible structure and allowed an efficient electron transfer between the electrode surface and the ferro/ferricyanide ($[Fe(CN)_6]^{3-/4-}$) redox probe in which the complexed Fe(III) is reduced to Fe(II): $Fe(CN)_6^{-3} + e^- = Fe(CN)_6^{-4}$.

After osteopontin binding, the aptamer conformation changes and forms a stable and rigid structure. This new conformation, blocks the electron transfer, resulting in a current decrease.

A change in the the experimental conditions, alters the current decrease. Indeed, under the experimental conditions of the first run (44°C, 1.5 µM of aptamer concentration, 20 min of aptamer incubation and 30 min of aptamer-osteopontin interaction) (Table 4.1), the peak of SWV and CV decreases slightly after the protein incubation which correspond to only 11% and 8% respectively for DNA aptamer and, 12% and 8% respectively for RNA aptamer.

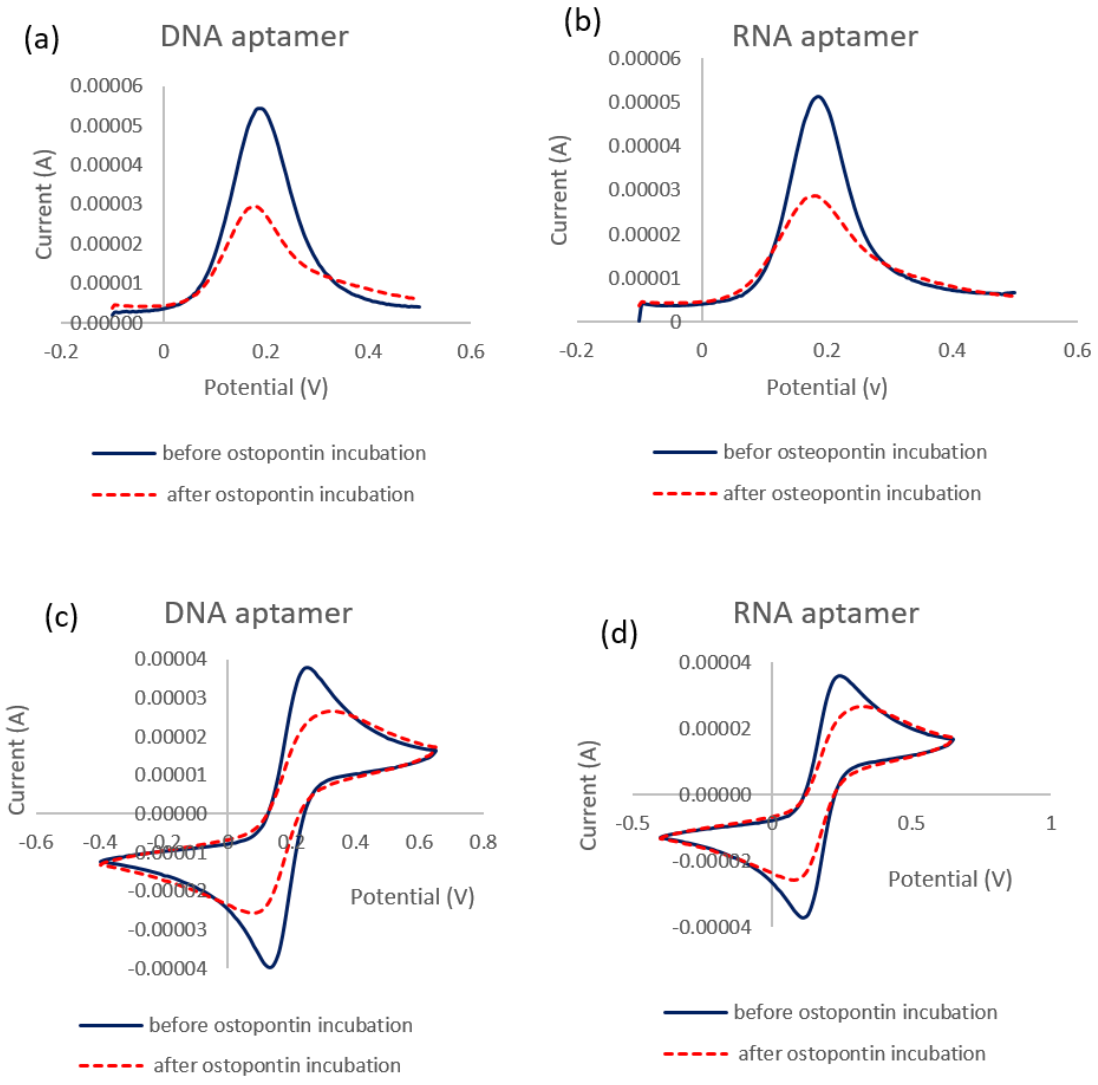

Figure 4.1: Square wave voltammetry response of (a) DNA aptamer and (b) RNA aptamer and cyclic voltammetry response for (c) DNA aptamer and (d) RNA aptamer.

4.2. Effect of the type of aptamer and electrochemical technique on the dual-aptasensor response

Besides estimating pure error and curvature, the center points allow analyzing the effect of the type of aptamer (RNA and DNA) and electrochemical technique (SWV and CV) on the dual-aptasensor array response because they are run in triplicate (run 6, 10 and 19 in Table 4.1). The relative current changes (ΔI %) relative to the center points are presented in Table 4.2.

The significance of the difference between the obtained responses is evaluated by the two-way analysis of variance (ANOVA). Table 4.3 shows a statistically significant difference in the response of the dual-aptasensor array based on the type of the electrochemical technique (p-value < 0.0001). This significant difference is only between SWV and CV_{ox} or SWV and CV_{red}. Both CV_{ox} and CV_{red} give similar responses. Because CV_{ox} and CV_{red} give similar responses, only the CV_{ox} will be considered for further analysis .These results confirm that SWV is more sensitive than CV. Indeed, it was reported that SWV allows detection limits as low as 10^{-8} M (Mendoza et al. 2015). The CV is more appropriate for the evaluation of the electrode surface such as its stability and purity and the cleaning of the electrode surface (Meirinho et al. 2015; Sethi 1994).

The responses of the dual-aptasensor array in term of type of aptamer were similar. Indeed, the results showed (Table 4.3) that there was no statistical significant differences between the electrochemical current changes recorded with the RNA and DNA aptamers (p-value = 0.529). This result reveals that DNA and RNA aptamers used had similar sensitivities and binding affinities towards osteopontin. These similar behaviors were expected since it has been reported that both complex DNA aptamer-osteopontin and RNA aptamer-osteopontin had similar dissociation constants (K_d of 2.5 nM and 1.6 nM respectively (Meirinho 2015; Mi et al. 2009)) after an incubation of 30 minutes . The two kinds of aptamer have in their sequences, at different sites, a stem-loop which is involved in the binding to the osteopontin protein. These stem-loop structures are important as binding regions of the DNA or RNA aptamers to their targets (Stoltenburg et al. 2007).

Finally, the interaction between type of aptamer and type of the electrochemical technique used had a p-value equal to 0.776 (Table 4.3) which indicates that this interaction has no statistical-significant effect on the electrochemical response of the aptasensors.

Table 4.2: Results (relative current changes ΔI %) relative to the center points of the experimental design

		Type of electrochemical technique		
		SWV[a]	CV[b] (ox)[c]	CV (red)[d]
Type of aptamer	DNA	32	13.6	13
		32.8	10.9	9.3
		37	13.7	11.3
	RNA	35	15.2	15.2
		32.4	10.8	10.7
		28	10.8	7.9

[a] square wave voltammetry; [b] cyclic voltammetry; [c] oxidation; [d] reduction

Table 4.3: Two way analysis of variance (ANOVA) of the results presented in Table 4.2

	Sum of Squares	df	Mean Square	F	Sig.
Type of aptamer	3.20	1	3.20	0.42	0.52
Type of electrochemical technique	1768.81	2	884.40	116.10	< 0.0001
Type of aptamer * type of electrochemical technique	3.95	2	1.97	0.25	0.77
Error	91.40	12	7.61	----	----
Total	8274.50	18	----	----	----

Pairwise comparison				
Type of electrochemical technique		Mean Difference	Std. Error	p-value
CV[a] (ox)[b]	CV (red)	-0.94	2.22	1.000
	SWV	-24.33	2.22	< 0.0001
CV (red)[c]	CV (ox)	0.94	2.22	1.000
	SWV	-23.39	2.22	< 0.0001
SWV[d]	CV (ox)	24.33	2.22	< 0.0001
	CV (red)	23.39	2.22	< 0.0001

[a] cyclic voltammetry; [b] oxidation; [d] square wave voltammetry; [c] reduction

4.3. Optimization of the experimental conditions

The main and interaction effects were calculated and are given in Table 4.4. Besides, the half-normal probability plots were also obtained using the software Design-Expert®. From the Table 4.4 it can be noticed that X_1 (aptamer concentration), X_3 (the

aptamer-protein interaction time) and X_4 (incubation temperature) have negative effects on the electrochemical current change response of the dual-aptasensor array regardless of the type of aptamer and electrochemical technique. This suggests that increasing X_1 and X_4 from the low level (0.5 µM, 30 min and 4°C, respectively) to the high level (1.5 µM, 90 min and 44°C, respectively) will decrease the response of the aptasensor. On the other hand, the effect of X_2 (immobilization time of the aptamer) is positive. This result means that the performance of the aptasensor increases when the factor passed from the low level (20 min) to the high level (60 min). However, the real meaning of the main effects may be limited if they are involved in significant interactions, which may turn out into misleading information, being therefore necessary to examine the statistical significant interactions.

Table 4.4: Calculated effect of the main and interaction effects

		ΔI_{SWV}^{DNA} [1]	ΔI_{SWV}^{RNA} [2]	ΔI_{CV}^{DNA} [3]	ΔI_{CV}^{RNA} [4]
Main effects	X_1	-4.32	-9.46	-3.02	-4.69
	X_2	8.12	7.70	1.26	2.59
	X_3	-0.29	-5.49	-1.02	-2.09
	X_4	-5.19	-7.71	-5.44	-4.53
Interaction effects	$X_1 X_2$	5.12	7.39	3.05	1.25
	$X_1 X_3$	4.85	3.34	2.56	1.42
	$X_1 X_4$	-3.12	-3.67	1.88	1.79
	$X_2 X_3$	-0.64	-2.33	2.62	0.18
	$X_2 X_4$	9.46	10.02	4.34	4.89
	$X_3 X_4$	7.49	-3.80	3.16	-2.07
	$X_1 X_2 X_3$	4.36	6.33	0.48	0.76
	$X_1 X_2 X_4$	2.36	11.57	-1.45	1.77
	$X_1 X_3 X_4$	-1.66	-3.00	-4.38	-3.79
	$X_2 X_3 X_4$	-9.50	-2.29	-3.16	0.18
	$X_1 X_2 X_3 X_4$	-0.63	0.17	0.82	0.16

[1] Relative current changes when using SWV as electrochemical technique and DNA as aptamer
[2] Relative current changes when using SWV as electrochemical technique and RNA as aptamer
[3] Relative current changes when using CV as electrochemical technique and DNA as aptamer
[4] Relative current changes when using CV as electrochemical technique and RNA as aptamer

In order to examine the magnitude of the factor effects, the pareto chart (Fig. 4.2) offers a simpler view of the relative effects. It is easy to notice from the pareto chart that the common most crucial effect for the four response (ΔI_{SWV}^{DNA} , $\Delta I_{SWV}^{RNA}, \Delta I_{CV}^{DNA}$ and ΔI_{CV}^{RNA}) is the interaction effect X_2 X_4 , whereas, the common least important effect is the interaction effect X_1 X_2 X_3 X_4. Effects that are likely to be important are selected from the half-normal probability plot generated by the software Design-Expert in order to create a significant model. Effects with no significance may be included to keep a hierarchical model. To confirm the validity of the model, analysis of variance (ANOVA) and diagnostic residuals were used (Table 4.5).

(a)

(b)

(c)

(d)

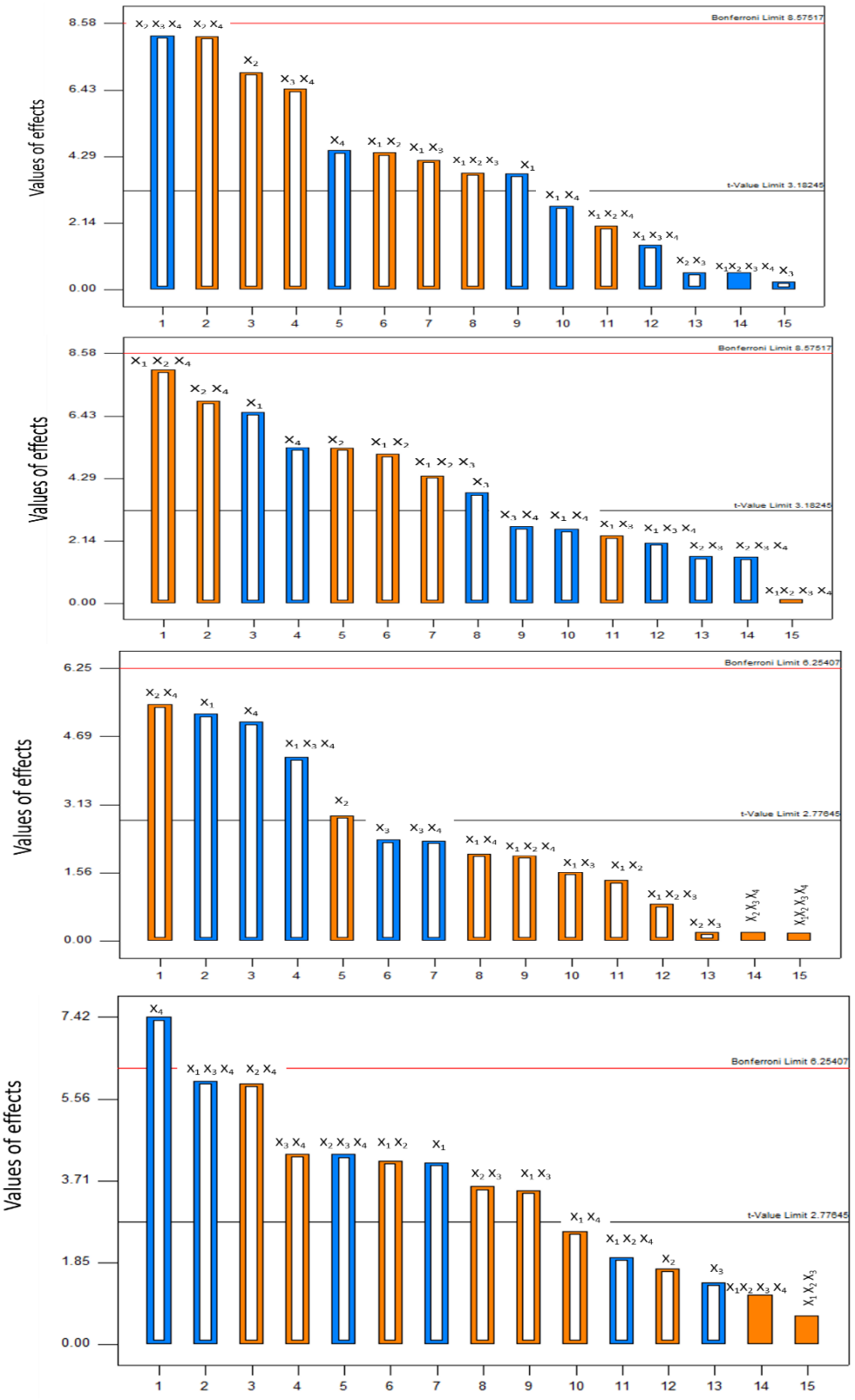

Figure 4.2: Pareto chart of effects for the responses (a) ΔI_{SWV}^{DNA}, (b) ΔI_{SWV}^{DNA} , (c) ΔI_{CV}^{RNA} and (d) ΔI_{CV}^{DNA}

Table 4.5: Analysis of variance (ANOVA) for the four created model and their diagnostic residuals

		SS	DF	MS	F-value	p-value
Model	ΔI_{SWV}^{DNA} [1]	1738.60	14.00	124.19	23.05	0.012
	ΔI_{SWV}^{RNA} [2]	2505.47	14.00	178.96	21.42	0.013
	ΔI_{CV}^{DNA} [3]	511.30	13.00	39.33	18.27	0.006
	ΔI_{CV}^{RNA} [4]	426.83	13.00	32.83	10.11	0.019
Curvature	ΔI_{SWV}^{DNA}	79.32	1.00	79.32	14.72	0.031
	ΔI_{SWV}^{RNA}	14.26	1.00	14.26	1.71	0.28
	ΔI_{CV}^{DNA}	9.58	1.00	9.58	4.45	0.10
	ΔI_{CV}^{RNA}	0.90	1.00	0.90	0.28	0.62
Residuals	ΔI_{SWV}^{DNA}	16.17	3.00	5.39	----	----
	ΔI_{SWV}^{RNA}	25.06	3.00	8.35	----	----
	ΔI_{CV}^{DNA}	8.61	4.00	2.15	----	----
	ΔI_{CV}^{RNA}	12.99	4.00	3.25	----	----
Lack of fit	ΔI_{SWV}^{DNA}	1.59	1.00	1.59	0.22	0.68
	ΔI_{SWV}^{RNA}	0.12	1.00	0.12	0.01	0.93
	ΔI_{CV}^{DNA}	3.58	2.00	1.79	0.71	0.58
	ΔI_{CV}^{RNA}	0.23	2.00	0.12	0.02	0.98
Pure error	ΔI_{SWV}^{DNA}	14.57	2.00	7.29	----	----
	ΔI_{SWV}^{RNA}	24.94	2.00	12.47	----	----
	ΔI_{CV}^{DNA}	5.04	2.00	2.52	----	----
	ΔI_{CV}^{RNA}	12.75	2.00	6.38	----	----

Models	R^2 [2]	$R^2_{adjusted}$	Q^2	Adequate precision
ΔI_{SWV}^{DNA}	0.99	0.94	0.74	19.51
ΔI_{SWV}^{RNA}	0.99	0.94	0.96	18.46
ΔI_{CV}^{DNA}	0.98	0.92	0.53	18.97
ΔI_{CV}^{RNA}	0.97	0.87	0.90	13.37

[1] Relative current changes when using SWV as electrochemical technique and DNA as aptamer
[2] Relative current changes when using SWV as electrochemical technique and RNA as aptamer
[3] Relative current changes when using CV as electrochemical technique and DNA as aptamer
[4] Relative current changes when using CV as electrochemical technique and RNA as aptamer

The four created models relative to the four responses (ΔI_{SWV}^{DNA}, ΔI_{SWV}^{RNA}, ΔI_{CV}^{DNA} *and* ΔI_{CV}^{RNA}) were found to be statistically significant (p-value= 0.0125; 0.0139; 0.0063 and 0.0191 respectively) and did not show lack-of-fit (p-value=0.6863; 0.9304; 0.5847 and 0.9822 respectively). In addition, they showed an acceptable determination coefficients (R^2 = 0.9907; 0.9900; 0.9834; 0.9704) that explain 99.07%, 99%, 98.34% and 97.04% of the response variability respectively, as well as a satisfactory adjusted determination coefficient ($R^2_{adjusted}$ = 0.9477; 0.9438; 0.9296 and 0.8745 respectively). Also, a satisfactory prediction determination coefficients were obtained (Q^2 = 0.7491; 0.9655;

0.5380 and 0.9010, respectively) showing that the prediction performance of the proposed models is acceptable. It is true that the prediction determination coefficients of the model relative to the response ΔI_{CV}^{DNA} is less than 0.6 but it can be considered as satisfactory Q^2 because the difference is very small. Moreover, the model showed an adequate precision (equal to 19.5155; 18.4672; 18.9792 and 13.3782, respectively), which means that the proposed models can be used to navigate the design space and for optimization purposes. The curvature of the model relative to the responses ΔI_{SWV}^{DNA} is significant (p-value 0.0312) which means that the values of the used center points are either higher or lower than those predicted by the factorial design. This indicates that the design is in the region of an optimum. The curvatures of the models relative to the responses ΔI_{SWV}^{RNA}, ΔI_{CV}^{DNA} and ΔI_{CV}^{RNA} are not significant (p-value = 0.2825, 0.1026, 0.6269, respectively) which means that the response of the dual-aptasensor array can be predicted by a first-order model equation:

$$\Delta I(\%) = \beta_0 + \sum_{i=1}^{4} \beta_i X_i + \sum_{i<j}^{6} \beta_{ij} X_i X_j + \sum_{i<j<k}^{3} \beta_{ijk} X_i X_j X_k + \beta_{1234} X_1 X_2 X_3.$$

The parameters (β's coefficient) of the regression model equations are shown in Table 4.6 and Table 4.7. The statistic analyses of the four created models do not reveal any problems so we can look at the significant factor effects in order to optimize the experimental condition of the dual-aptasensor array.

Table 4.6: Regression parameters (for the coded factors) of the two models for the responses ΔI_{SWV}^{DNA} and ΔI_{SWV}^{DNA}

Coded factors	Model parameters (eq 2.3)	ΔI_{SWV}^{DNA} (%) [1]		ΔI_{SWV}^{RNA}(%) [2]	
		β's coefficient	p-value	β's coefficient	p-value
Intercept	β_0	39.54		34.19	
X_1	β_1	-2.16	0.03	-4.73	0.007
X_2	β_2	4.06	0.006	3.85	0.032
X_3	β_3	-0.15	0.81	-2.74	0.01
X_4	β_4	-2.60	0.02	-3.86	0.01
X_1 X_2	β_{12}	2.56	0.02	3.70	0.1
X_1 X_3	β_{13}	2.42	0.02	1.67	0.01

Table 4.6 (continued)

$X_1 X_4$	β_{14}	-1.56	0.07	-1.84	0.08
$X_2 X_3$	β_{23}	-0.32	0.62	-1.16	0.20
$X_2 X_4$	β_{24}	4.73	0.003	5.01	0.07
$X_3 X_4$	β_{34}	3.75	0.007	-1.90	0.006
$X_1 X_2 X_3$	β_{123}	2.18	0.03	3.16	0.02
$X_1 X_2 X_4$	β_{124}	1.18	0.13	5.79	0.12
$X_1 X_3 X_4$	β_{134}	-0.83	0.24	-1.50	0.004
$X_2 X_3 X_4$	β_{234}	-4.75	0.003	-1.14	0.21
$X_1 X_2 X_3 X_4$	β_{1234}	----	----	----	----

[1] Relative current changes when using SWV as electrochemical technique and DNA as aptamer
[2] Relative current changes when using SWV as electrochemical technique and RNA as aptamer

Table 4.7: Regression parameters (for the coded factors) of the two models for the responses ΔI_{CV}^{DNA} and ΔI_{CV}^{DNA}

Coded factors	Model parameters (eq 2.3)	ΔI_{CV}^{DNA} (%)[1]		ΔI_{CV}^{RNA}(%)[2]	
		β's coefficient	p-value	β's coefficient	p-value
Intercept	β_0	14.68	----	12.86	----
X_1	β_1	-1.51	0.01	-2.35	0.006
X_2	β_2	0.63	0.16	1.3	0.04
X_3	β_3	-0.51	0.23	-1.04	0.08
X_4	β_4	2.72	0.001	-2.27	0.007
$X_1 X_2$	β_{12}	1.52	0.01	0.63	0.23
$X_1 X_3$	β_{13}	1.28	0.02	0.71	0.18
$X_1 X_4$	β_{14}	0.94	0.06	0.9	0.11
$X_2 X_3$	β_{23}	1.31	0.02	0.088	0.85
$X_2 X_4$	β_{24}	2.17	0.004	2.44	0.005
$X_3 X_4$	β_{34}	1.58	0.01	-1.03	0.08
$X_1 X_2 X_3$	β_{123}			0.38	0.44
$X_1 X_2 X_4$	β_{124}	-0.72	0.11	0.88	0.12
$X_1 X_3 X_4$	β_{134}	-2.19	0.003	-1.9	0.01
$X_2 X_3 X_4$	β_{234}	-1.58	0.01	----	----
$X_1 X_2 X_3 X_4$	β_{1234}	----	----	----	----

[1] Relative current change when using CV as electrochemical technique and DNA as aptamer
[2] Relative current change when using CV as electrochemical technique and RNA as aptamer

The X_1 X_2, X_1 X_4, and X_2 X_4 interactions are the key to solving the problem of optimization. The X_1X_2 interaction for the four models (ΔI_{SWV}^{DNA}, ΔI_{SWV}^{RNA}, ΔI_{CV}^{DNA} and ΔI_{CV}^{RNA} are plotted in the Fig. 4.3 which show how the aptamer concentration and time of immobilization of the aptamer interact to affect the response of the aptasensor. Two lines appear on the plots, bracketed by least significant difference (LSD) bars at either end. The lines are far from parallel, indicating quite different effects of changing the concentration of aptamer (X_1). In Fig. 4.3 ((a) and (b)) the line is almost flat when the immobilization time is high (X_2 = 60 min), which indicates that the system is unaffected by aptamer concentration. In Fig. 4.3 ((c) and (d)), when the immobilization time is set at its high level, the change in aptasensor response is also small. However, when the time is at the low level, the line angles decreases indicating a strong negative effect due to the increased aptamer concentration. The combination of high concentration and low time is bad for the response. When the aptamer concentration is set at its low level (X_1 = 0.5 µM), the response remains high regardless of the time setting. In fact, the LSD bars overlap at this end of the interaction graph, which implies that there is no significant difference in the aptasensor response. From this interaction (X_1 X_2), we conclude that the best response would appear to be obtained when: X_1 and X_2 are both at the high level or when X_1 at the low level regardless of X_2 level. The second solution is definitely better than the first one, especially when the immobilization time is set at the low level because it allows a reduction in the operational costs and time. However, we have to check if the immobilization time at its high level induces or not a better response when interacting with other factors.

Fig. 4.4 exhibit the same pattern of again the nonparallel lines that are characteristic of a powerful two-factor interaction. The effect of immobilization time on the aptasensor response depends on the level of temperature, represented by the two lines on the graph. On the top line, the least significant difference (LSD) bars overlap from left to right which indicates that at low temperature (X_4 = 4°C), there is not much, if any, effect. However, the aptasensor response differs for the lower line on the graphs where incubation temperature is set at its high level (X_4 = 44°C). Here the LSD bars do not overlap, indicating that the effect of immobilization time is significant. In fact, when the time is at its low level, the temperature has the largest effect on aptasensor response among all the other factors whereas; it has not a significant effect when the time is at its high level. In fact, incubation temperature has little effect at high time but the largest effect on the

aptasensor response at low immobilization time. Therefore, the best aptasensor response for this interaction is reached when X_2 and X_4 are set at the low level or when the time is at its high level regardless of the temperature level.

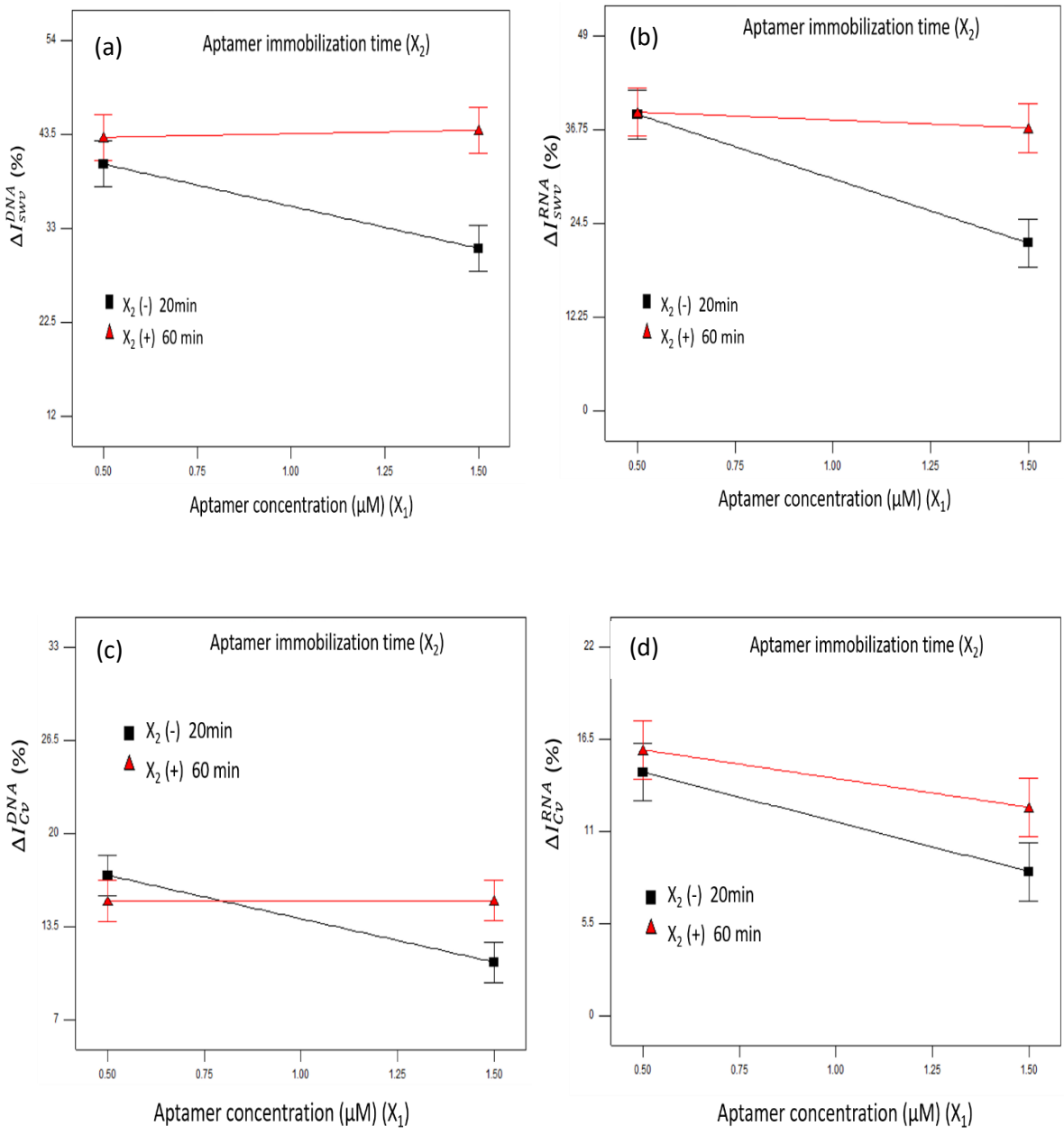

Figure 4.3: Interaction graphs of factors X_1 (aptamer concentration) versus X_2 (aptamer immobilization time) for the responses (a) ΔI_{SWV}^{DNA}, (b) ΔI_{SWV}^{DNA} , (c) ΔI_{CV}^{DNA} and (d) ΔI_{CV}^{RNA}

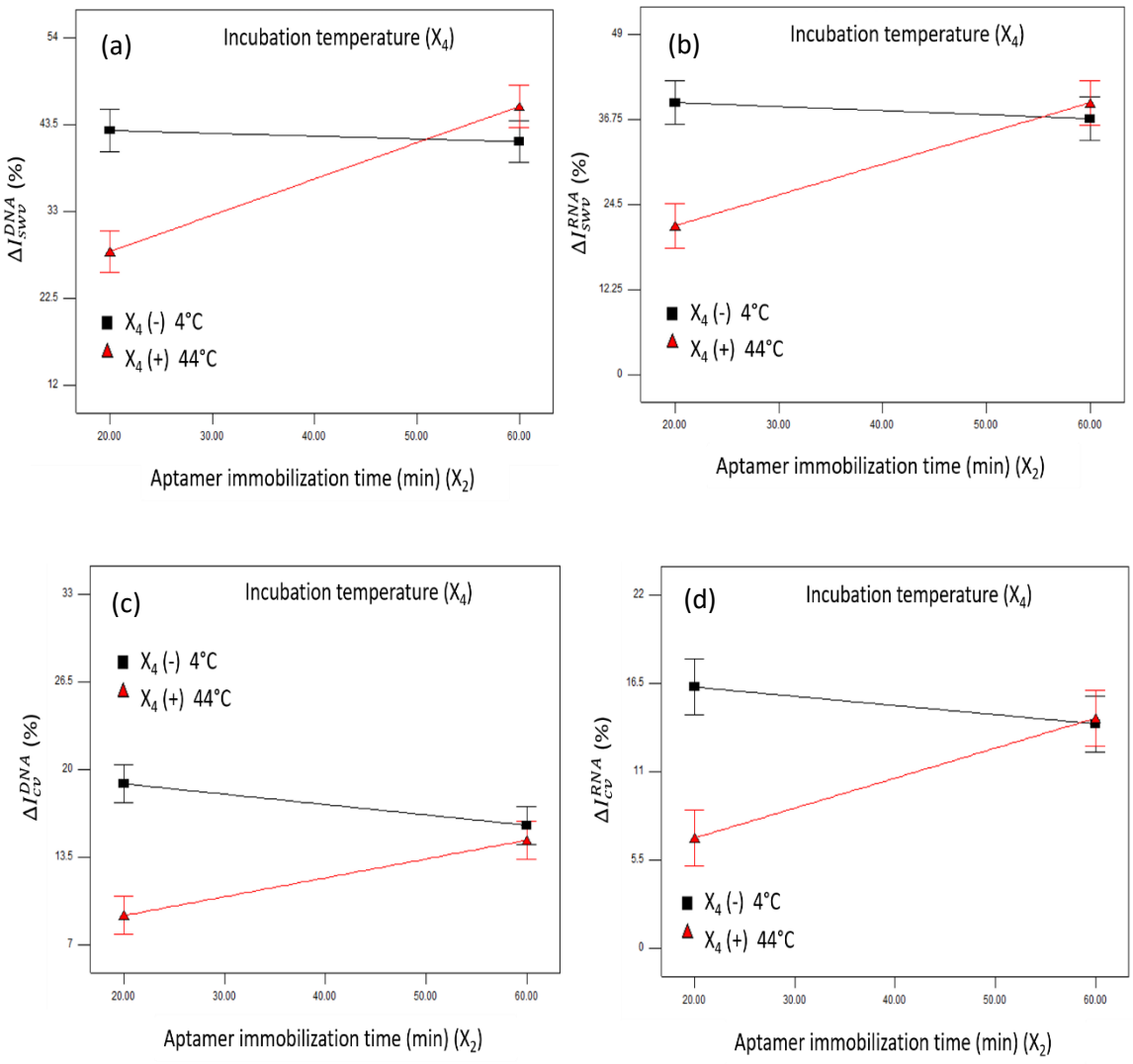

Figure 4.4: Interaction graphs of factors X_2 (aptamer immobilization time) versus X_4 (incubation temperature) for the responses (a) ΔI_{SWV}^{DNA}, (b) ΔI_{SWV}^{DNA} , (c) ΔI_{CV}^{DNA} and (d) ΔI_{CV}^{RNA}

From the interaction X_1X_4 (Fig. 4.5 (c) and (d)), we note that the spread of the points on the right side of the graph (where aptamer concentration is high) is smaller than the spread between the points at the left side of the graph (where aptamer concentration is low.) In other words, the effect of temperature is less significant at the high level of X_1. Therefore, the combination of low temperature and low aptamer concentration gives the best response. Whereas the best results in Fig. 4.5 ((a) and (b)) are obtained when the concentration is also at its low level regardless of the temperature.

For the interaction X_3X_4 (Fig. 4.6), DNA and RNA aptamers do not exhibit the same pattern of interaction. In fact, for the DNA aptamer (Fig. 4.6 (a) and (c)) the best response is achieved when X_3 and X_4 are both at their low levels. When the temperature is set at

the high level, an increase in the interaction time between aptamer and osteopontin improve slightly the response. However, for the RNA aptamer (Fig. 4.6 (b) and (d)), an increase in the interaction time between aptamer and osteopontin when the temperature is set at the high level, deteriorate the response. In this case, the best result is obtained when the temperature is at its low level regardless of the interaction time or when the interaction time is low and the temperature is high.

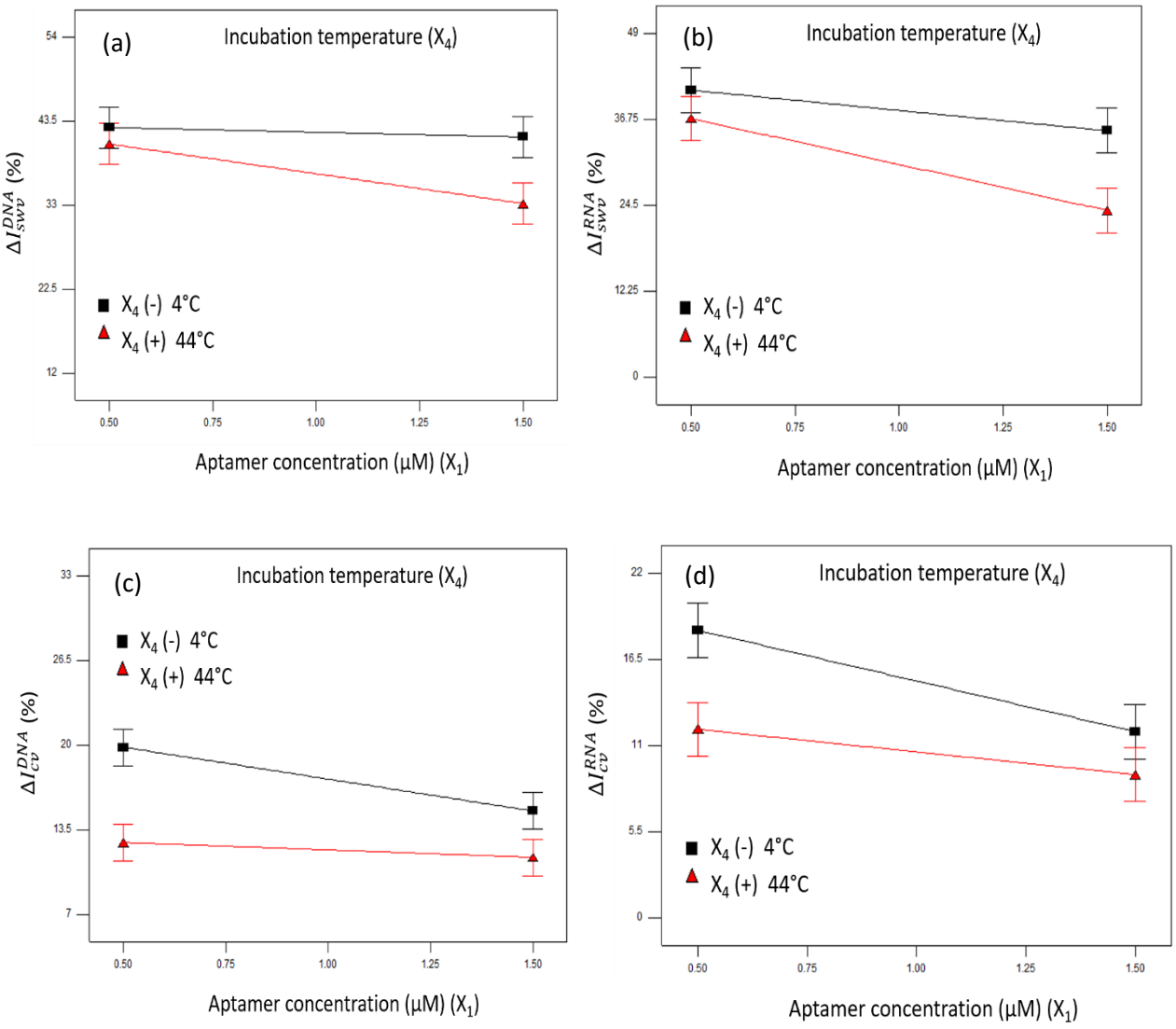

Figure 4.5: Interaction graphs of factors X_1 (aptamer concentration) versus X_4 (incubation temperature) for the responses (a) ΔI_{SWV}^{DNA}, (b) ΔI_{SWV}^{DNA} , (c) ΔI_{CV}^{DNA} and (d) ΔI_{CV}^{RNA}

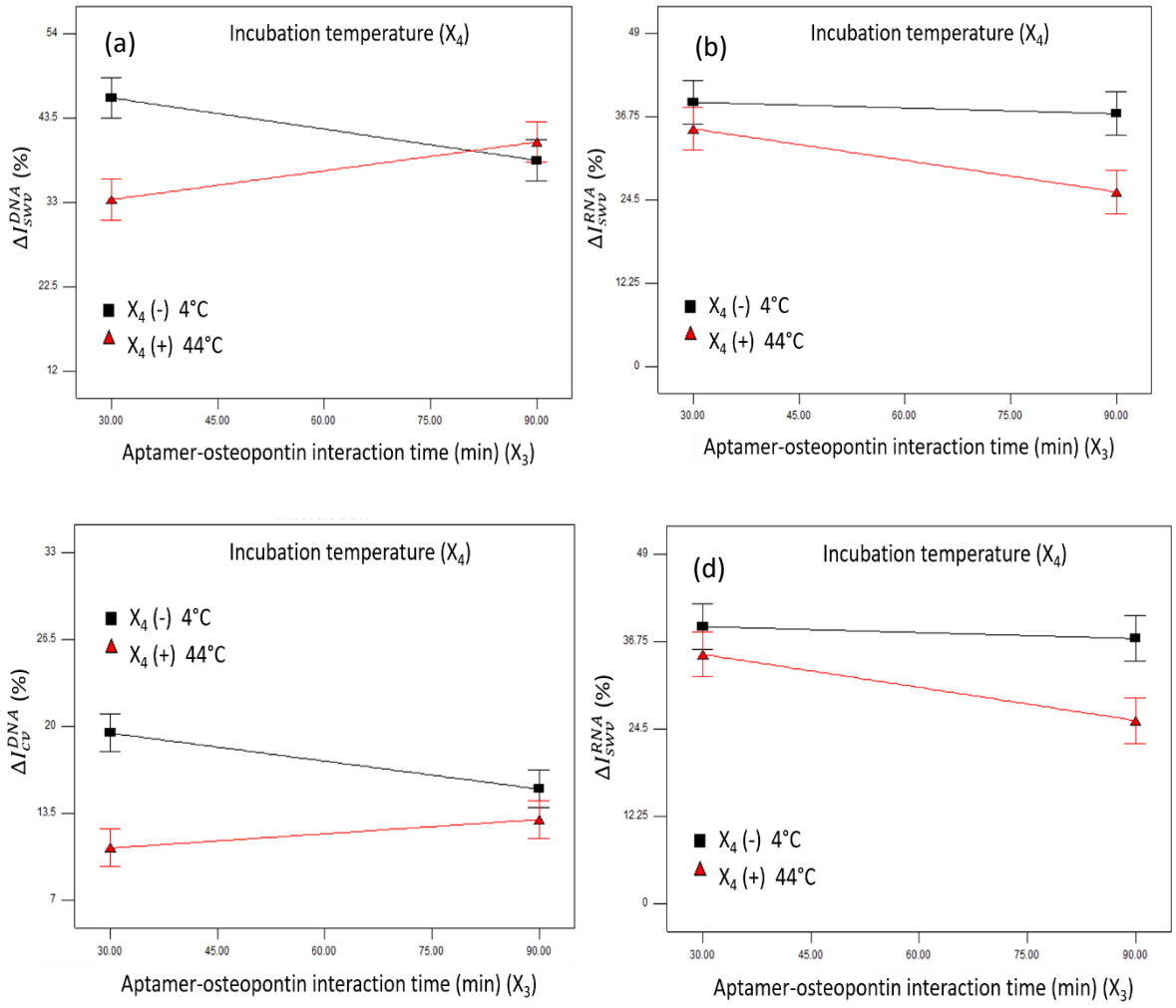

Figure 4.6: Interaction graphs of factors X_3 (interaction time between aptamer and osteopontin) versus X_4 (incubation temperature) for the responses (a) ΔI_{SWV}^{DNA}, (b) ΔI_{SWV}^{DNA} , (c) ΔI_{CV}^{DNA} and (d) ΔI_{CV}^{RNA}

Taking into account all the analyzed interactions, we conclude that the combination of low aptamer concentration, low time of aptamer immobilization, low interaction time between aptamer and osteopontin and low incubation temperature enhances the performance of the aptasensor with the main advantage of reducing operational costs and time. Under these conditions, an electrochemical current changes of 54%, 41%, 32% and 22% in ΔI_{SWV}^{DNA}, ΔI_{SWV}^{RNA} and ΔI_{CV}^{DNA} respectively were obtained which corresponds to an improvement of about 56%, 24%, 50% and 23% respectively comparing to the values of single aptasensor (aptamer concentration: 0.4µM; incubation temperature: 24°C; interaction time between aptamer and protein: 60 min; aptamer immobilization time: 40 min), previously reported in the literature (Meirinho et al. 2015; Meirinho 2016).

However, it is worth noting that the surface of the WE used in the single aptasensor is smaller than the WE used for the developed dual-aptasensor. In addition, an improvement of about 61% and 12% in ΔI_{CV}^{DNA} and ΔI_{CV}^{RNA} respectively was achieved comparing to the reported values of a dual-aptasensor operating under non-optimized experimental conditions (aptamer concentration: 0.4µM; incubation temperature: 24°C; interaction time between aptamer and protein: 60 min; aptamer immobilization time: 40 min) (Meirinho 2016).

The 3 D surface graphs (Fig. 4.7) show the common best experimental conditions for the 4 four responses ΔI_{SWV}^{DNA} , ΔI_{SWV}^{RNA}, ΔI_{CV}^{DNA} *and* ΔI_{CV}^{RNA} that allow enhancing the performance of the developed electrochemical dual-aptasensor array.

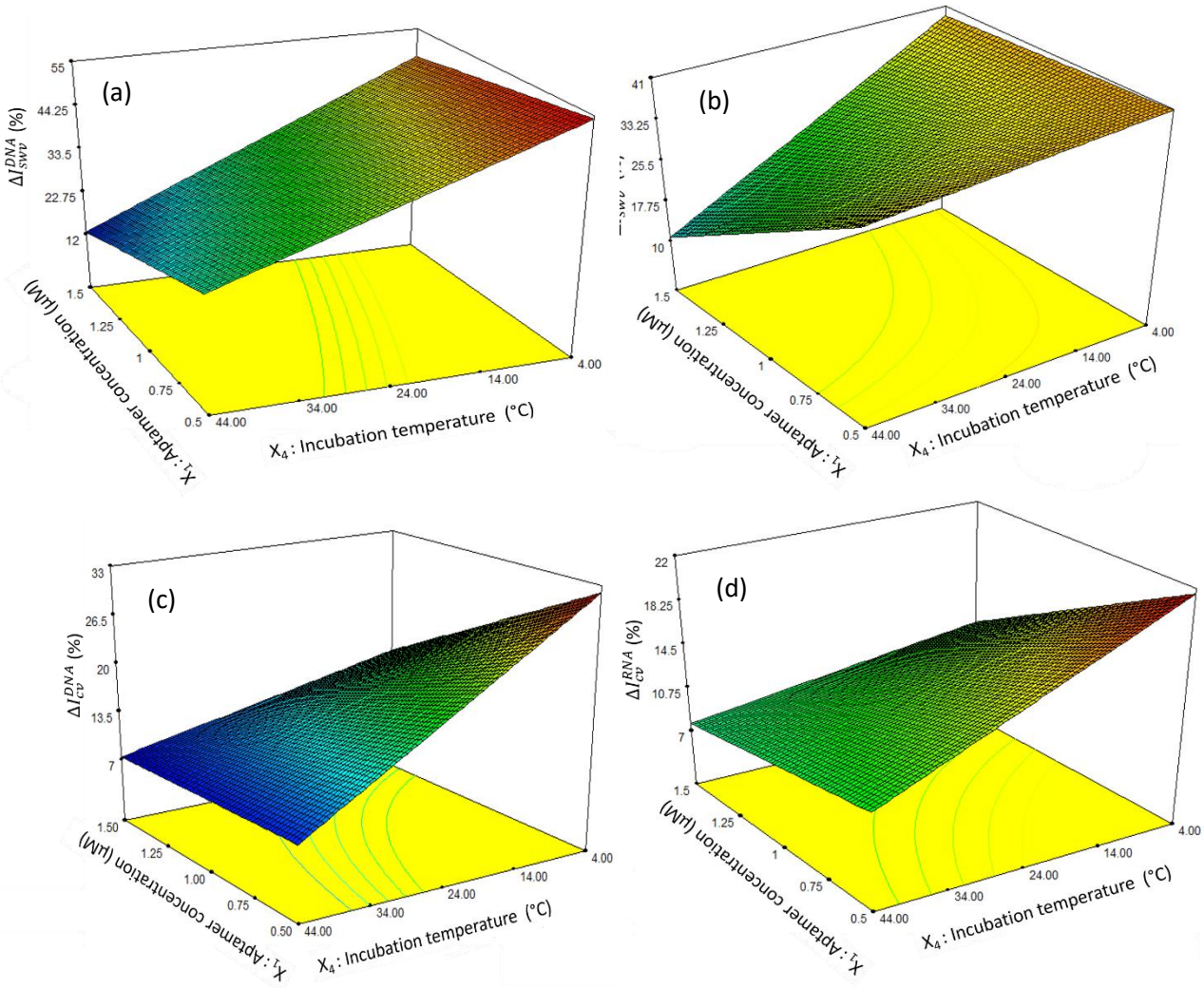

Figure 4.7: 3 D surface graphs of the optimal experimental conditions for the responses ΔI_{SWV}^{DNA}, (b) ΔI_{SWV}^{DNA} , (c) ΔI_{CV}^{DNA} and (d) ΔI_{CV}^{RNA} at 20 min of aptamer incubation and 30 min of aptamer-osteopontin interaction.

CHAPTER 5

Conclusion and future perspectives

In this work, an electrochemical dual-aptasensor array was built for the possible early detection of cancer. The effects of four operating experimental conditions (aptamer concentration, time of aptamer immobilization into dual-screen printed gold electrodes (Dual-SPGE), the aptamer-protein interaction time and incubation temperature) and of their interactions on the signal response of the developed dual-aptasensor were experimentally investigated using two electrochemical techniques, namely the SWV and CV.

The modeling and optimization of the signal response of the developed dual-aptasensor array was satisfactorily performed using a 2^k factorial design methodology that allowed establishing the optimal experimental conditions that enabled enhancing the electrochemical current change of the signal response.

The results obtained showed that the established models can be used to predict the signal response of the aptasensor under any given conditions within the experimental range studied (aptamer concentration from 0.5 µM to 1.5 µM, incubation temperature from 4°C to 44°C, time of aptamer immobilization between 20 min and 60 min and time of aptamer-osteopontin interaction between 30 min and 90 min). Temperature and aptamer concentration were found to be the most significant parameters. In addition, under the optimized experimental conditions an effective enhancement of the signal response was achieved. A 53.86% and 41% in ΔI_{SWV}^{DNA} and ΔI_{SWV}^{RNA} respectively were obtained in experiment conducted under the optimized experimental conditions (aptamer concentration of 0.5 µM for both DNA and RNA aptamers; an incubation temperature of 4ºC; 20 min aptamer immobilization time into the Dual-SPGE at 4ºC; and aptamer-protein interaction time of 30 min).

Since the preliminary experimental design performed pointed out that the optimized experimental conditions were at their low level, a new factorial design with a reduced number of factors should be tested in order to verify if the signal response could be further improved. From the results already obtained, the new design will be a reduced one with only three factors since it would not be feasible to carried out assays at temperatures lower than 4°C, otherwise the working solutions may freeze. For ΔI_{SWV}^{DNA}, a significant curvature was detected. Therefore, the 2^k factorial design should be augmented into a response surface methodology based on a rotable central composite design by locating new points along the axes of the factor space.

Finally, this study can be seen as a useful input and an effective contribution for the development of more performant aptasensor since statistical design of experiments have been only applied in a few studies.

References

Aghahosseini, S., Dincer, I. & Naterer, G.F., 2013. Linear sweep voltammetry measurements and factorial design model of hydrogen production by HCl/CuCl electrolysis. *International Journal of Hydrogen Energy*, 38, pp.12704–12717.

Ahmed, M. et al., 2011. Osteopontin: a potentially important therapeutic target in cancer. *Expert opinion on therapeutic targets*, 15, pp.1113–26.

AlcheikhHamdon, A.A., Darwish, N.A. & Hilal, N., 2015. The use of factorial design in the analysis of air-gap membrane distillation data. *Desalination*, 367, pp.90–102.

Anderson, M.J., Whitcomb, P.J., 2013. DOE Simplified: Practical Tools for Effective Experimentation, *Journal of Chemical Information and Modeling*, 53, pp.1689–1699.

Arya, S. K., Singh, P. S. and Malhotra, B.D., 2007. Electrochemical Techniques in Biosensors. *Handbook of biosensors and biochips*, pp.342-377.

Bai, H.Y., Campo, F.J. del & Tsai, Y.C., 2013. Sensitive electrochemical thrombin aptasensor based on gold disk microelectrode arrays. *Biosensors and Bioelectronics*, 42, pp.17–22.

Bhatt, A.N. et al., 2010. Cancer biomarkers - current perspectives. *The Indian journal of medical research*, 132, pp.129–149.

Bosco, F.G. et al., 2013. Micromechanical PDGF recognition via lab-on-a-disc aptasensor arrays. *Sensors and Actuators A: Physical*, 195, pp.154–159.

Bramwell, V.H.C. et al., 2014. Assessment of osteopontin in early breast cancer: correlative study in a randomised clinical trial. *Breast cancer research*, 16, pp.1-10.

Cao, X. et al., 2017. A new dual-signalling electrochemical aptasensor with the integration of "signal on/off" and "labeling/label-free" strategies. *Sensors and Actuators B: Chemical*, 239, pp.166–171.

Chatziharalambous, D. et al., 2016. Analytical performance of ELISA assays in Urine: One more bottleneck towards biomarker validation and clinical implementation. *PLoS ONE*, 11, pp.1–12.

Cheng, A.K.H., Sen, D. & Yu, H.Z., 2009. Design and testing of aptamer-based electrochemical biosensors for proteins and small molecules. *Bioelectrochemistry*, 77, pp.1–12.

Clapp RW, Howe GK, Jacobs MM., 2005 Lowell Center for Sustainable Production. Environmental and occupational causes of cancer a review of recent scientific literature. pp.1-29.

Collins, A.L. et al., 2012. Osteopontin expression is associated with improved survival in patients with pancreatic adenocarcinoma. *Annals of surgical oncology*, 19, pp.2673–2978.

Dominguez, A. et al., 2012. New improved method for fructooligosaccharides production by Aureobasidium pullulans. *Carbohydrate Polymers*, 89, pp.1174–1179.

Duan, N. et al., 2016. Advances in aptasensors for the detection of food contaminants. *The Analyst*, 141, pp.3942–3961.

Elhalil, A. et al., 2016. Factorial experimental design for the optimization of catalytic degradation of malachite green dye in aqueous solution by Fenton process. *Water Resources and Industry*, 15, pp.41–48.

Farghaly, O. A, Hameed, R.S.A. & Abu-Nawwas, A.-A.H., 2014. Analytical Application Using Modern Electrochemical Techniques. *International Journal of Electrochemical Science*, 9, pp.3287–3318.

Feng, X. et al., 2015. A novel "dual-potential" electrochemiluminescence aptasensor array using CdS quantum dots and luminol-gold nanoparticles as labels for simultaneous detection of malachite green and chloramphenicol. *Biosensors and Bioelectronics*, 74, pp.587–593.

Feng, X. et al., 2016. Ratiometric electrochemiluminescent aptasensor array for antibiotic based on internal standard method and spatial-resolved technique. *Sensors and Actuators B: Chemical*, 226, pp.305–311.

Ferreira, L.B. et al., 2016. Osteopontin-a splice variant is overexpressed in papillary thyroid carcinoma and modulates invasive behavior. *Oncotarget*, 7, pp.52003-520016.

Fischer, L.M. et al., 2009. Gold cleaning methods for electrochemical detection applications. *Microelectronic Engineering*, 86, pp.1282–1285.

Gam, L.-H., 2012. Breast cancer and protein biomarkers. *World Journal of Experimental Medicine*, 2, pp.86–91.

Gan, S.D. & Patel, K.R., 2013. Enzyme immunoassay and enzyme-linked immunosorbent assay. *The Journal of Investigative Dermatology*, 133, pp.1-3.

Gold, L. et al., 2010. Aptamer-based multiplexed proteomic technology for biomarker discovery. *PLoS ONE*, 5, pp.1-17.

Goossens, N., Nakagawa, S., Sun, X., Hoshida, Y., 2015. Cancer biomarker discovery and validation. *Translational Cancer Research*, 4, pp.256–269.

Grieshaber, D. et al., 2008. Electrochemical Biosensors - Sensor Principles and Architectures. *Sensors*, 8, pp.1400–14580.

Han, K., Liang, Z. & Zhou, N., 2010. Design strategies for aptamer-based biosensors. *Sensors*, 10, pp.4541–4557.

Hao, C. et al., 2016. Prognostic Value of Osteopontin Splice Variant-c Expression in Breast Cancers: A Meta-Analysis. *BioMed Research International*, 2016, pp.1–8.

Harris, C.C., 2015. Cause and prevention of human cancer. *Carcinogenesis*, 36, pp.S1.

Henry, N.L. & Hayes, D.F., 2012. Cancer biomarkers. *Molecular Oncology*, 6, pp.140-146.

Hsu, K.-H. et al., 2010. Osteopontin expression is an independent adverse prognostic factor in resectable gastrointestinal stromal tumor and its interaction with CD44 promotes tumor proliferation. *Annals of Surgical Oncology*, 17, pp.3043–3052.

Huang, J., Hu, W. & Sood, A.K., 2010. Prognostic Biomarkers in Ovarian Cancer. *National Institutes of Health*, 8, pp.231–251.

Huang, R. et al., 2016. Role of Osteopontin in the Carcinogenesis and Metastasis of Colorectal Cancer. *Journal of Cancer Therapy*, 7, pp.729–740.

Khang, H. et al., 2017. All-in-one dual-aptasensor capable of rapidly quantifying carcinoembryonic antigen. *Biosensors and Bioelectronics*, 90, pp.46–52.

Kothari, A.N. et al., 2016. Osteopontin — A Master Regulator of Epithelial-Mesenchymal Transition. *Journal of Cancer Therapy*, 5, pp.1-16.

Kraatz, H.-B. & Amini, K., 2015. Recent Developments in Biosensor Technologies for Pathogen Detection in Water. *JSM Environmental Science & Ecology*, 3, pp.1–9.

Lau, P. et al., 2009. NMP22 is predictive of recurrence in high-risk superficial bladder cancer patients. *Journal of the Canadian Urological Association*, 3, pp.454–458.

Lee, E.Y.H.P. & Muller, W.J., 2010. Oncogenes and tumor suppressor genes. *Cold Spring Harbor Perspectives in Biology*, 2, pp.1–18.

Lehman, T.A. et al., 1991. Oncogenes and tumor-suppressor genes. *Environmental Health Perspectives*, 93, pp.133–144.

Li, C. et al., 2016. Improvement of enzyme-linked immunosorbent assay for the multicolor detection of biomarkers. *Chemical Science*, 7, pp.3011–3016.

Liang, Y. et al., 2011. Elevated circulating levels of osteopontin are associated with metastasis in advanced non-small cell lung cancer. *Chinese Journal of Cancer Research*, 23, pp.64–68.

Liersch, R. et al., 2015. Osteopontin is a prognostic factor for survival of acute myeloid leukemia patients. *Blood*, 119, pp.5215–5221.

Lowe, C.R., 2008. Overview of Biosensor and Bioarray Technologies. Handbook of Biosensors and Biochips, pp.1-16

Macrì, A. et al., 2009. Role of osteopontin in breast cancer patients. *Tumori*, 95, pp.48–52.

Matušan-Ilijaš, K. et al., 2011. Osteopontin expression correlates with nuclear factor-κB activation and apoptosis downregulation in clear cell renal cell carcinoma. *Pathology - Research and Practice*, 207, pp.104–110.

Mehrotra, P., 2016. Biosensors and their applications - A review. *Journal of Oral Biology and Craniofacial Research*, 6, pp.153–159.

Meirinho, S.G. et al., 2015. Development of an electrochemical RNA-aptasensor to detect human osteopontin. *Biosensors and Bioelectronics*, 71, pp.332–341.

Meirinho, S.G., 2016. Development of a novel aptamer-based multi-sensor device for the detection of osteopontin. Doctoral thesis, University of Minho, Braga, Portugal, pp.1-184.

Mi, Z. et al., 2009. RNA Aptamer Blockade of Osteopontin Inhibits Growth and Metastasis of MDA-MB231 Breast Cancer Cells. *Molecular Therapy*, 17, pp.153–161.

Mirza, M. et al., 2008. Osteopontin-c is a selective marker of breast cancer. International *Journal of Cancer*, 122, pp.889–897.

Misek, D.E. & Kim, E.H., 2011. Protein biomarkers for the early detection of breast cancer. *International Journal of Proteomics*, 2011, p.343-582.

Mishra, A. & Verma, M., 2010. Cancer biomarkers: Are we ready for the prime time? *Cancers*, 2, pp.190–208.

Montgomery, D., 2001. Design and Analysis of Experiments. Jhon Wiley & Sons, Inc, 5th, p.684.

Moreno, M., 2014. Aptasensors. Encyclopedia of Astrobiology. Springer-Verlag Berlin Heidelberg, pp.1-3.

Nassar, H.R. et al., 2015. Prognostic significance of plasma osteopontin level in breast cancer patients. *Forum of Clinical Oncology*, 6, pp.27–32.

Neta, N.S. et al., 2011. Maximization of fructose esters synthesis by response surface methodology. *New Biotechnology*, 28, pp.349–355.

Newman, J.D. & Turner, 2007. Historical Perspective of Biosensor and Biochip Development. Handbook of Biosensors and Biochips. John Wiley & Sons, Ltd. pp.1-16.

Nimse, S.B. alasaheb et al., 2014. Immobilization techniques for microarray: challenges and applications. *Sensors*, 14, pp.22208–22229.

Ozer, A., Pagano, J.M. & Lis, J.T., 2014. New Technologies Provide Quantum Changes in the Scale, Speed, and Success of SELEX Methods and Aptamer Characterization. *Molecular therapy - Nucleic Acids*, 3, pp.1-18.

Psyrri, A. et al., 2017. Association of osteopontin with specific prognostic factors and survival in adjuvant breast cancer trials of the Hellenic Cooperative Oncology Group. *Journal of Translational Medicine*, 15, pp.1–11.

Radi, A.-E. & Abd-Elgawad, 2011. Electrochemical Aptamer-Based Biosensors: Recent Advances and Perspectives. *International Journal of Electrochemistry*, 2011, pp.1–17.

Rangaswami, H., Bulbule, A. & Kundu, G.C., 2006. Osteopontin: Role in cell signaling and cancer progression. *Trends in Cell Biology*, 16, pp.79–87.

Rhouati, A. et al., 2016. Label-Free Aptasensors for the Detection of Mycotoxins. *Sensors*, 16, pp.1-21.

Rittling, S.R. & Chambers, A.F., 2004. Role of osteopontin in tumour progression. *British Journal of Cancer*, 90, pp.1877–1881.

Ry, A.K.F. z et al., 2013. Translation of proteomic biomarkers into FDA approved cancer diagnostics: issues and challenges. *Clinical Proteomics*, 10, pp.1-14.

Salem, M. et al., 2013. Clinical Significance of Plasma Osteopontin Level as a Biomarker of Hepatocellular Carcinoma. *Gastroenterology Research*, 6, pp.191–199.

Sase, S.P., Ganu, J. V & Nagane, N., 2012. Osteopontin : A Novel Protein Molecule. *Indian Medical Gazette*, February, pp.62–66.

Sethi, R.S., 1994. Transducer aspects of biosensors. *Biosensors and Bioelectronics*, 9, pp.243–264.

Shevde, L.A. & Samant, R.S., 2014. Role of osteopontin in the pathophysiology of cancer. *Matrix Biology*, 37, pp.131–141.

Shojaei, F. et al., 2012. Osteopontin induces growth of metastatic tumors in a preclinical model of non-small lung cancer. *Journal of Experimental and Clinical Cancer Research*, 31, pp.1-12.

Sivakumar, S. & Niranjali Devaraj, S., 2014. Tertiary structure prediction and identification of druggable pocket in the cancer biomarker – Osteopontin-c. *Journal of Diabetes & Metabolic Disorders*, 13, pp.1-14.

Song, W. et al., 2014. Disposable electrochemical aptasensor array by using in situ DNA hybridization inducing silver nanoparticles aggregate for signal amplification. *Analytical Chemistry*, 86, pp.2775–2783.

Srivastava, S., Verma, M. & Gopal-Srivastava, R., 2005. Proteomic maps of the cancer-associated infectious agents. *Journal of Proteome Research*, 4, pp.1171–1180.

Stoltenburg, R., Reinemann, C. & Strehlitz, B., 2007. SELEX-A (r)evolutionary method to generate high-affinity nucleic acid ligands. *Biomolecular Engineering*, 24, pp.381–403.

Taleat, Z., Khoshroo, A. & Mazloum-Ardakani, M., 2014. Screen-printed electrodes for biosensing: A review (2008-2013). *Microchimica Acta*, 181, pp.865–891.

Ugo, P. & Moretto, L.M., 2016. A Low-Cost Label-Free AFB1 Impedimetric Immunosensor Based on Functionalized CD-Trodes. *Chemosensors*, 4, pp 1-10.

Vigneshvar, S. et al., 2016. Recent Advances in Biosensor Technology for Potential Applications - An Overview. *Frontiers in Bioengineering and Biotechnology*, 4, pp.1-9.

Webber Stones, T. C. et al., 2014. Proteomics Analysis of Cancer Exosomes Using a Novel Modified Aptamer-based Array (SOMAscanTM) Platform. *Molecular & Cellular Proteomics*, 13, pp.1050–1064.

Weber, G.F., Lett, G.S. & Haubein, N.C., 2010. Osteopontin is a marker for cancer aggressiveness and patient survival. *British Journal of Cancer*, 103, pp.861–869.

Wood, R. et al., 2001. Human DNA repair genes. *Science*, 291, pp.1284–1289.

Yamanaka, K., Vestergaard, M.C. & Tamiya, E., 2016. Printable electrochemical biosensors: A focus on screen-printed electrodes and their application. *Sensors*, 16, pp.1–16.